Computable bounds of functional outputs in linear visco-elastodynamics

Francesc Verdugo[a,1], Pedro Díez[a,b,2,*]

[a] *Universitat Politècnica de Catalunya (UPC)*
Laboratori de Càlcul Numèric (LaCàN)
Jordi Girona 1-3 E-08034 Barcelona, Spain
[b] *Centre Internacional de Mètodes Numèrics en Enginyeria, (CIMNE)*
Gran Capitán s/n, E-08034 Barcelona, Spain

Abstract

This work presents a new technique yielding computable bounds of quantities of interest in the framework of linear visco-elastodynamics. A novel expression for the error representation is introduced, alternative to the previous ones using the Cauchy-Schwarz inequality. The proposed formulation utilizes symmetrized forms of the error equations to derive error bounds in terms of energy error measures. The practical implementation of the method is based on constructing admissible fields for both the original problem and the adjoint problem associated with the quantity of interest. Here, the flux-free technique is considered to compute the admissible stress fields. The proposed methodology yields estimates with better quality than the ones based on the Cauchy-Schwarz inequality. In the studied examples the bound gaps obtained are approximately halved, that is the estimated intervals of confidence are reduced.

Keywords: computable bounds, quantity of interest, adjoint problem, goal-oriented error assessment, visco-elastodynamics.

1. Introduction

The pioneering works discussing error estimators for elliptic problems [1, 2, 3] introduced techniques assessing the energy norm of the error in Finite Element Analysis. These tools are essential to assess the reliability of numerical simulations and they are

*Corresponding author
[1] E–mail: francesc.verdugo@upc.edu
[2] E–mail: pedro.diez@upc.edu

also a key ingredient for subsequent strategies providing more meaningful error measures [4, 5, 6, 7]. The latter, aiming at assessing arbitrary functional outputs of the solution describing some *quantity of interest*, are referred as *goal-oriented* error estimators.

Error estimates for elliptic (steady state) problems have reached an amazing degree of maturity, with different techniques providing excellent error estimates in an extensive collection of model problems. The error estimation tools dealing with transient problems are not so popular, especially in the case of structural dynamics. Some of the contributions on this last topic are, on the one hand, the energy error estimates presented by Aubry *et al.* [8], Li and Wiberg [9, 10] and Ladevèze *et al.* [11, 12, 13, 14] and, on the other hand, the goal-oriented estimates proposed by Schleupen and Ramm [15], Fuentes *et al.* [16] and Ladevèze and co-workers [17, 18, 19, 20].

Interest has been paid also to the error assessment tools providing bounds, that is yielding one-sided estimates (both lower bounds guaranteeing that the error is underestimated and upper bounds guaranteeing that the error is overestimated) . This topic has been addressed recently in many references, see for instance [5] where Parés *et al.* propose bounds of linear outputs for the linear elastic case. The estimates providing bounds have also been extended to transient problems, see for instance [21] where the transient convection-diffusion-reaction equation is considered. To the best knowledge of the authors, the only references discussing bounds in a quantity of interest for linear visco-elastodynamics are due to Ladevèze and co-workers [17, 18, 19, 20].

The present work aims at finding an alternative error representation improving the estimates introduced in [18]. The strategy presented in [18] is briefly revisited, using an algebraic rationale without the requirement of any thermodynamic framework. In order to simplify the developments, a linear Kelvin-Voigt constitutive relation is considered here, instead of the Maxwell model. This allows a simpler derivation, using only algebraic arguments, with no need of any mechanical consideration. Generalization to nonlinear models would require a general thermodynamical framework.

The proposed method describes how to compute lower and upper bounds of a linear output $L^{\mathcal{O}}(\mathbf{u})$ of the exact solution $\mathbf{u}$, namely ζ_{L} and ζ_{U} such that $\zeta_{\mathrm{L}} \leq L^{\mathcal{O}}(\mathbf{u}) \leq \zeta_{\mathrm{U}}$. The novel contribution of this work is the introduction of an alternative expression for values ζ_{L} and ζ_{U}. This new expression reduces the bound gap: with respect to the existing technique based on the Cauchy-Schwarz inequality, the bound gap is approximately halved. The basic rationale is similar to the one considered for linear elasticity. Bounds for the quantity of interest are obtained as a proper combination of bounds for a global energy measure of both the original and the adjoint problems. The key ingredient is the computation of admissible fields for both problems. An other novelty with respect to [18] is the utilization of the flux-free technique [22] in order to build the admissible stress fields.

The remainder of this article is organized as follows. Section 2 introduces the equations of visco-elastodynamics and its numerical approximation with the Newmark method. Section 3 is devoted to obtain upper bounds of energy error measures. Section 4 discusses how to obtain bounds in quantities of interest following the error representation presented in [18]. Section 5 introduces the new error representation leading to better bounded estimates. Section 6 contains the numerical examples. The paper is closed with some concluding remarks.

2. Problem statement

2.1. Governing equations

A visco-elastic body occupies the open bounded domain $\Omega \subset \mathbb{R}^d$, $d \leq 3$, with boundary $\partial\Omega$. The boundary is divided in two disjoint parts, Γ_{N} and Γ_{D} such that $\partial\Omega = \overline{\Gamma_{\mathrm{N}}} \cup \overline{\Gamma_{\mathrm{D}}}$. The time interval under consideration is $I := [0, T]$. Under the assumption of small perturbations, the evolution of displacements $\mathbf{u}(\mathbf{x}, t)$ and stresses $\boldsymbol{\sigma}(\mathbf{x}, t)$, $\mathbf{x} \in \Omega$ and $t \in I$, is described by the visco-elastodynamic equations,

$$\rho\ddot{\mathbf{u}} - \boldsymbol{\nabla} \cdot \boldsymbol{\sigma} = \mathbf{f} \quad \text{in } \Omega \times I, \tag{1a}$$

$$\mathbf{u} = \mathbf{0} \quad \text{on } \Gamma_{\mathrm{D}} \times I, \tag{1b}$$

$$\boldsymbol{\sigma} \cdot \mathbf{n} = \mathbf{g} \quad \text{on } \Gamma_{\mathrm{N}} \times I, \tag{1c}$$

$$\mathbf{u} = \mathbf{u}_0 \quad \text{at } \Omega \times \{0\}, \tag{1d}$$

$$\dot{\mathbf{u}} = \mathbf{v}_0 \quad \text{at } \Omega \times \{0\}, \tag{1e}$$

where $\rho = \rho(\mathbf{x}) > 0$ is the mass density and an upper dot indicates partial derivation with respect to time, that is $\dot{(\bullet)} := \frac{\mathrm{d}}{\mathrm{d}t}(\bullet)$. The body force is denoted by $\mathbf{f}$, $\mathbf{g}$ is the traction acting on the Neumann boundary $\Gamma_{\mathrm{N}} \times I$ and $\mathbf{n}$ is the outward unit normal to $\partial\Omega$. Functions $\mathbf{u}_0 = \mathbf{u}_0(\mathbf{x})$ and $\mathbf{v}_0 = \mathbf{v}_0(\mathbf{x})$ are the initial conditions for displacements and velocities respectively. For the sake of simplicity and without any loss of generality, Dirichlet conditions (1b) are taken as homogeneous, see Appendix A for details. The set of equations (1) is closed with the constitutive law,

$$\boldsymbol{\sigma} := \boldsymbol{\mathcal{C}} : \boldsymbol{\varepsilon}(\mathbf{u} + \tau\dot{\mathbf{u}}), \tag{2}$$

corresponding to the Kelvin-Voigt linear visco-elastic model. The parameter $\tau > 0$ is a characteristic time related with the amount of viscosity of the medium. The introduction of this parameter is fundamental in obtaining bounds. For $\tau = 0$ the bounding properties are lost. The tensor $\boldsymbol{\mathcal{C}}$ is the standard 4th-order elastic Hooke tensor. The kinematic relation (corresponding to small perturbations) $\boldsymbol{\varepsilon}(\mathbf{w}) := \frac{1}{2}(\boldsymbol{\nabla}\mathbf{w} + \boldsymbol{\nabla}^T\mathbf{w})$ is considered.

In the following it is useful to rewrite the constitutive relation (2) as

$$\boldsymbol{\sigma} := \mathbf{s}(\mathbf{u}) = \mathbf{s}^{\mathrm{E}}(\mathbf{u}) + \mathbf{s}^{\nu}(\mathbf{u}),$$

where

$$\mathbf{s}^{\mathrm{E}}(\mathbf{w}) := \boldsymbol{\mathcal{C}} : \boldsymbol{\varepsilon}(\mathbf{w}), \tag{3a}$$
$$\mathbf{s}^{\nu}(\mathbf{w}) := \tau\boldsymbol{\mathcal{C}} : \boldsymbol{\varepsilon}(\dot{\mathbf{w}}). \tag{3b}$$

The following notation is introduced for the elastic and viscous part of the stress $\boldsymbol{\sigma}$ respectively:

$$\boldsymbol{\sigma}^{\mathrm{E}} := \mathbf{s}^{\mathrm{E}}(\mathbf{u}), \tag{4a}$$
$$\boldsymbol{\sigma}^{\nu} := \mathbf{s}^{\nu}(\mathbf{u}). \tag{4b}$$

Remark 1. *The following analysis can be generalized for other more sophisticated linear Kelvin-Voigt models. These models can be introduced taking alternative expressions for* $\mathbf{s}^{\nu}$ *in equation* (3b)*. This would lead to a technical modification in the definition of the bilinear forms* B^{ν} *and* $\bar{B}^{\nu}$ *introduced in equations* (13) *and* (14b) *below. Note however that the main rationale of the methodology presented in the paper is straightforwardly generalized to deal with more complex visco-elastic models.*

The subsequent analysis requires introducing a variational version of problem (1). To this end, the following spaces are introduced

$$\boldsymbol{\mathcal{W}} := \left\{ \mathbf{w} : \begin{array}{ll} \mathbf{w}(\mathbf{x},\cdot) \in [H^2(I)]^d & \forall \mathbf{x} \in \Omega \\ \mathbf{w}(\cdot,t) \in [H^1(\Omega)]^d & \forall t \in I \\ \mathbf{w} = \mathbf{0} & \text{at } \Gamma_{\mathrm{D}} \times I \end{array} \right\},$$

and

$$\boldsymbol{\mathcal{U}} := \left\{ \mathbf{w} \in \boldsymbol{\mathcal{W}} : \begin{array}{ll} \mathbf{w} = \mathbf{u}_0 & \text{at } \Omega \times \{0\} \\ \dot{\mathbf{w}} = \mathbf{v}_0 & \text{at } \Omega \times \{0\} \end{array} \right\}.$$

Functions in $\boldsymbol{\mathcal{U}}$ are said to be *kinematically admissible* or *K-admissible*. They are continuous in space-time with continuous time derivative and they fulfill the initial and Dirichlet conditions. The variational version of (1) reads: find $\mathbf{u} \in \boldsymbol{\mathcal{U}}$ such that

$$B(\mathbf{u},\mathbf{w}) = L(\mathbf{w}) \quad \forall \mathbf{w} \in \boldsymbol{\mathcal{W}}, \tag{5}$$

where

$$B(\mathbf{v},\mathbf{w}) := \int_I (\rho\ddot{\mathbf{v}},\dot{\mathbf{w}})\ \mathrm{d}t + \int_I a(\mathbf{v}+\tau\dot{\mathbf{v}},\dot{\mathbf{w}})\ \mathrm{d}t, \tag{6a}$$

$$L(\mathbf{w}) := \int_I l(\dot{\mathbf{w}})\ \mathrm{d}t, \tag{6b}$$

$$l(\mathbf{w}) := (\mathbf{f},\mathbf{w}) + (\mathbf{g},\mathbf{w})_{\Gamma_\mathrm{N}}, \tag{6c}$$

$$(\mathbf{v},\mathbf{w}) := \int_\Omega \mathbf{v}\cdot\mathbf{w}\ \mathrm{d}\Omega, \tag{6d}$$

$$(\mathbf{v},\mathbf{w})_{\Gamma_\mathrm{N}} := \int_{\Gamma_\mathrm{N}} \mathbf{v}\cdot\mathbf{w}\ \mathrm{d}\Gamma, \tag{6e}$$

$$a(\mathbf{v},\mathbf{w}) := \int_\Omega \boldsymbol{\varepsilon}(\mathbf{v}) : \boldsymbol{\mathcal{C}} : \boldsymbol{\varepsilon}(\mathbf{w})\ \mathrm{d}\Omega. \tag{6f}$$

A numerical solution of the original problem (1) may be found without using this time-space variational setting. Nevertheless, the variational formulation is useful in the following to assess the error and, in particular, in order to obtain error bounds.

2.2. Numerical approximation

The well known Newmark method [23] is considered for the numerical approximation of problem (1). The Newmark method is chosen because it is commonly used in practical applications and commercial codes. Note however that the present study is applicable to other semidiscrete methods and straightforwardly generalizable to space-time formulations, for instance those introduced by Hughes and Hulbert [24, 25]. In fact, taking as reference methodology the Newmark or other semidiscrete methods is actually more involved than the space-time ones. This is because they combine finite elements and finite differences and therefore the discrete solution cannot take advantage of variational properties. However, this drawback can be easily overcomed as it is shown later.

As previously noted, The Newmark and other semidiscrete methods are based on a FE discretization in space and finite differences in time. Thus, a variational setting in space for each $t \in I$ is required. The following space has to be introduced:

$$\boldsymbol{\mathcal{V}}_0 := \left\{ \mathbf{w} \in [H^1(\Omega)]^d : \mathbf{w} = \mathbf{0} \text{ on } \Gamma_\mathrm{D} \right\}.$$

Equations (1) are rewritten as: for all $t \in I$ find $\mathbf{u}(\cdot,t) \in \boldsymbol{\mathcal{V}}_0$ such that

$$(\rho\ddot{\mathbf{u}}(\cdot,t),\mathbf{w}) + a(\mathbf{u}(\cdot,t)+\tau\dot{\mathbf{u}}(\cdot,t),\mathbf{w}) = l(\mathbf{w}) \quad \forall \mathbf{w} \in \boldsymbol{\mathcal{V}}_0, \tag{7}$$

with initial conditions $\mathbf{u}(\cdot,t) = \mathbf{u}_0$ and $\dot{\mathbf{u}}(\cdot,t) = \mathbf{v}_0$. After discretization in $\boldsymbol{\mathcal{V}}_0^H \subset \boldsymbol{\mathcal{V}}_0$ (H stands for the characteristic mesh element size) equation (7) leads to a system of second

order ODEs, which is discretized in time introducing the following partition of the time interval I,

$$\mathcal{T} := \{t_0 = 0, t_1, \cdots, t_N = T\}.$$

Each interval of the partition $\mathcal{T}$ is characterized by the time step $\Delta t_n := t_n - t_{n-1}$. The characteristic time step for the partition is taken as the maximum: $\Delta t := \max_n(\Delta t_n)$.

The proposed methodology is applicable to any method producing fields $\mathbf{u}_n^{rnisH,\Delta t}$, $\mathbf{v}_n^{H,\Delta t}$, $\mathbf{a}_n^{H,\Delta t} \in \boldsymbol{\mathcal{V}}_0^H$ for $n = 0, \cdots, N$ such that they fulfill the following condition

$$(\rho \mathbf{a}_n^{H,\Delta t}, \mathbf{w}) + a(\mathbf{u}_n^{H,\Delta t} + \tau \mathbf{v}_n^{H,\Delta t}, \mathbf{w}) = l_n(\mathbf{w}) \quad \forall \mathbf{w} \in \boldsymbol{\mathcal{V}}_0^H, \tag{8}$$

where

$$\begin{aligned} l_n(\mathbf{w}) &:= (\mathbf{f}_n, \mathbf{w}) + (\mathbf{g}_n, \mathbf{w})_{\Gamma_N}, \\ \mathbf{f}_n(\mathbf{x}) &:= \mathbf{f}(\mathbf{x}, t_n), \\ \mathbf{g}_n(\mathbf{x}) &:= \mathbf{g}(\mathbf{x}, t_n), \end{aligned}$$

and the initial conditions $\mathbf{u}_0^{H,\Delta t} = \mathbf{u}_0$ and $\mathbf{v}_0^{H,\Delta t} = \mathbf{v}_0$.

Note that the solution provided by the Newmark method complies with this requirement. In fact, the Newmark solution at time t_n is computed injecting the Taylor expansions

$$\begin{aligned} \mathbf{u}_n^{H,\Delta t} &= \mathbf{u}_{n-1}^{H,\Delta t} + \Delta t_n \mathbf{v}_{n-1}^{H,\Delta t} + \frac{1}{2}\Delta t_n^2 \left[(1-2\beta)\mathbf{a}_{n-1}^{H,\Delta t} + 2\beta \mathbf{a}_n^{H,\Delta t}\right], \\ \mathbf{v}_n^{H,\Delta t} &= \mathbf{v}_{n-1}^{H,\Delta t} + \Delta t_n \left[(1-\gamma)\mathbf{a}_{n-1}^{H,\Delta t} + \gamma \mathbf{a}_n^{H,\Delta t}\right], \end{aligned}$$

in equation (8) and assuming that the values $\mathbf{u}_{n-1}^{H,\Delta t}, \mathbf{v}_{n-1}^{H,\Delta t}, \mathbf{a}_{n-1}^{H,\Delta t}$ are known. The displacements and velocities at time t_0 are determined by the initial conditions $\mathbf{u}_0$ and $\mathbf{v}_0$, and the acceleration $\mathbf{a}_0^{H,\Delta t}$ is build such that

$$(\rho \mathbf{a}_0^{H,\Delta t}, \mathbf{w}) + a(\mathbf{u}_0 + \tau \mathbf{v}_0, \mathbf{w}) = l_0(\mathbf{w}) \quad \forall \mathbf{w} \in \boldsymbol{\mathcal{V}}_0^H.$$

The scalars β and γ are the parameters of the Newmark method taking values in $[0, 1]$.

Note that the fields $\mathbf{u}_n^{H,\Delta t}$, $\mathbf{v}_n^{H,\Delta t}$, $\mathbf{a}_n^{H,\Delta t}$ do not define functions in the whole time interval I, but only in the time partition. However, they can be extended to the interior

of the time steps using a simple linear interpolation:

$$\mathbf{u}^{H,\Delta t}(\mathbf{x},t) := \sum_{n=0}^{N} \mathbf{u}_n^{H,\Delta t}(\mathbf{x})\theta_n(t), \tag{9a}$$

$$\mathbf{v}^{H,\Delta t}(\mathbf{x},t) := \sum_{n=0}^{N} \mathbf{v}_n^{H,\Delta t}(\mathbf{x})\theta_n(t), \tag{9b}$$

$$\mathbf{a}^{H,\Delta t}(\mathbf{x},t) := \sum_{n=0}^{N} \mathbf{a}_n^{H,\Delta t}(\mathbf{x})\theta_n(t), \tag{9c}$$

where functions $\theta_n(t)$ $n = 0, \cdots, N$ are piecewise linear shape functions related with the time partition $\mathcal{T}$.

2.3. Interpretation of the damping factor

Before going further, it is worth analyzing the physical meaning of the parameter τ. This parameter is fundamental in the obtention of the bounds. The amount of damping associated with τ is characterized by the so-called adimensional damping factor denoted by ξ. For the Kelvin-Voigt model presented in equation (2), ξ has the following expression (see [18] for details):

$$\xi := \frac{1}{2}\tau\omega_0,$$

where $\omega_0 := \sqrt{\lambda_0}$, being λ_0 the lowest eigenvalue of the following generalized eigenvalue problem: find $\lambda \in \mathbb{R}$ and $\mathbf{q} \in \boldsymbol{\mathcal{V}}_0$ such that

$$a(\mathbf{q},\mathbf{w}) = \lambda(\rho\mathbf{q},\mathbf{w}),\ \forall \mathbf{w} \in \boldsymbol{\mathcal{V}}_0. \tag{10}$$

The value $\xi = 0\%$ corresponds to pure elasticity whereas $\xi = 100\%$ means that all vibration modes of the problem are dumped out. In the latter case, the corresponding solution is a pure decaying exponential. In practice, the eigenvalue λ_0 is approximated using the discrete space $\boldsymbol{\mathcal{V}}_0^H \subset \boldsymbol{\mathcal{V}}_0$ which results in the generalized eigenvalue problem

$$\mathbf{K}\mathbf{q} = \lambda\mathbf{M}\mathbf{q},$$

where $\mathbf{K}, \mathbf{M}$ are the stiffness and mass matrices corresponding with the forms in (10).

3. Constitutive relation error: Upper bound of energy error measures

3.1. Discretization error

Note that the numerical solution provided by the Newmark method, namely $\mathbf{u}^{H,\Delta t}, \mathbf{v}^{H,\Delta t}$ and $\mathbf{a}^{H,\Delta t}$, is such that the velocities are not the time derivatives of the displacements and accelerations are not the time derivatives of the velocities. Moreover, Their time dependence is not regular enough to fit in the variational setup described in equation (5), that is $\mathbf{u}^{H,\Delta t} \notin \boldsymbol{\mathcal{U}}$. A new displacement field $\hat{\mathbf{u}} \in \boldsymbol{\mathcal{U}}$ is introduced as a postprocess of the Newmark solution in order to analyze the corresponding error using the variational setup. The detailed construction of $\hat{\mathbf{u}}$ is described in section 3.5. In the remainder of the paper, the error analysis is referred to the approximate solution $\hat{\mathbf{u}}$.

The error associated with $\hat{\mathbf{u}}$, namely

$$\hat{\mathbf{e}} := \mathbf{u} - \hat{\mathbf{u}}, \tag{11}$$

lives in the space

$$\boldsymbol{\mathcal{U}}_0 := \left\{ \mathbf{w} \in \boldsymbol{\mathcal{W}} : \quad \begin{array}{ll} \mathbf{w} = \mathbf{0} & \text{at } \Omega \times \{0\} \\ \dot{\mathbf{w}} = \mathbf{0} & \text{at } \Omega \times \{0\} \end{array} \right\},$$

and fulfills the variational residual equation: find $\hat{\mathbf{e}} \in \boldsymbol{\mathcal{U}}_0$ such that

$$B(\hat{\mathbf{e}}, \mathbf{w}) = \hat{R}(\mathbf{w}) \quad \forall \mathbf{w} \in \boldsymbol{\mathcal{W}}, \tag{12}$$

where

$$\hat{R}(\mathbf{w}) := L(\mathbf{w}) - B(\hat{\mathbf{u}}, \mathbf{w}).$$

Note that the residual $\hat{R}$ does not verify the Galerkin orthogonality property because in general for arbitrary $\hat{\mathbf{u}} \in \boldsymbol{\mathcal{U}}$ and $\mathbf{w} \in \boldsymbol{\mathcal{W}}$, $B(\hat{\mathbf{u}}, \mathbf{w}) \neq L(\mathbf{w})$.

3.2. Energy measures

The first step to achieve bounds of the error $\hat{\mathbf{e}}$ in a quantity of interest is obtaining bounds of this error in a suitable energy measure. The measure to be used is associated with the following symmetric bilinear form

$$B^{\nu}(\mathbf{v}, \mathbf{w}) := \tau \int_I a(\mathbf{v}, \mathbf{w}) \, \mathrm{d}t. \tag{13}$$

Remark 2. *The form B^{ν} is related with the symmetric part of the form B, i.e.*

$$\frac{1}{2}\left[B(\mathbf{v}, \mathbf{w}) + B(\mathbf{w}, \mathbf{v})\right] = \frac{1}{2}\left[(\rho\dot{\mathbf{v}}, \dot{\mathbf{w}}) + a(\mathbf{v}, \mathbf{w})\right]_{t=0}^{t=T} + B^{\nu}(\mathbf{v}, \mathbf{w}).$$

Note that B^ν coincides with the dissipative term of the symmetric part of B, hence the superscript "ν" is used in B^ν marking its relation with the viscosity. The difference between B^ν and the symmetric part of B are the terms defined at times $t = 0$ and $t = T$ which are not related with the viscosity. Note that the higher is the value τ, the closer B^ν and the symmetric part of B are.

It is useful defining equivalent versions of forms a and B^ν taking stresses as arguments:

$$\bar{a}(\boldsymbol{\tau}_1, \boldsymbol{\tau}_2) := (\boldsymbol{\tau}_1, \boldsymbol{\mathcal{C}}^{-1} : \boldsymbol{\tau}_2), \tag{14a}$$

$$\bar{B}^\nu(\boldsymbol{\tau}_1, \boldsymbol{\tau}_2) := \frac{1}{\tau} \int_I \bar{a}(\boldsymbol{\tau}_1, \boldsymbol{\tau}_2) \, \mathrm{d}t. \tag{14b}$$

The relations $a(\mathbf{v}, \mathbf{w}) = \bar{a}(\mathbf{s}^{\mathrm{E}}(\mathbf{v}), \mathbf{s}^{\mathrm{E}}(\mathbf{w}))$ and $B^\nu(\mathbf{v}, \mathbf{w}) = \bar{B}^\nu(\mathbf{s}^\nu(\mathbf{v}), \mathbf{s}^\nu(\mathbf{w}))$ hold for all $\mathbf{v}$ and $\mathbf{w}$. The bilinear forms B^ν and $\bar{B}^\nu$ lead to the energy measures:

$$\|\mathbf{w}\|^2 := B^\nu(\mathbf{w}, \mathbf{w}) = \tau \int_I \|\dot{\mathbf{w}}\|^2 \, \mathrm{d}t,$$

$$\|\boldsymbol{\tau}\|_\sigma^2 := \bar{B}^\nu(\boldsymbol{\tau}, \boldsymbol{\tau}) = \frac{1}{\tau} \int_I \|\boldsymbol{\tau}\|_\sigma^2 \, \mathrm{d}t,$$

where $\|\mathbf{w}\|^2 := a(\mathbf{w}, \mathbf{w})$ and $\|\boldsymbol{\tau}\|_\sigma^2 := \bar{a}(\boldsymbol{\tau}, \boldsymbol{\tau})$. Note that the notation introduced above is such that norms with subscript "σ" and bilinear forms with upper bar take stresses as arguments.

Remark 3. *The bilinear form B is not symmetric but it is related with the following energy measure*

$$B(\mathbf{v}, \mathbf{v}) = \frac{1}{2} \left[|\dot{\mathbf{v}}|^2 + \|\mathbf{v}\|^2 \right]_{t=0}^{t=T} + \|\mathbf{v}\|^2, \tag{15}$$

which corresponds to the increment of the free energy (kinetic and elastic) plus the dissipated energy due to the viscosity. Note that the dissipated energy coincides with the energy related to the bilinear form B^ν. In particular for $\mathbf{v} = \hat{\mathbf{e}}$ one has

$$B(\hat{\mathbf{e}}, \hat{\mathbf{e}}) \geq \|\hat{\mathbf{e}}\|^2. \tag{16}$$

This relation is derived from (15) *noting that $\hat{\mathbf{e}}(0) = \dot{\hat{\mathbf{e}}}(0) = \mathbf{0}$ and $|\dot{\hat{\mathbf{e}}}|_{t=T}^2 + \|\hat{\mathbf{e}}\|_{t=T}^2 \geq 0$. The relation* (16) *is important because it is used later to derive bounds in the quantity of interest.*

3.3. Admissible fields

The construction of an admissible pair $(\hat{\boldsymbol{\sigma}}, \hat{\mathbf{u}}) \in \boldsymbol{\mathcal{S}}(\hat{\mathbf{u}}) \times \boldsymbol{\mathcal{U}}$ is the key ingredient in order to obtain upper bounds of the energy of $\hat{\mathbf{e}}$. The space of admissible stresses $\boldsymbol{\mathcal{S}}(\hat{\mathbf{u}})$ is defined for a given $\hat{\mathbf{u}} \in \boldsymbol{\mathcal{U}}$ as follows

$$\boldsymbol{\mathcal{S}}(\hat{\mathbf{u}}) := \left\{ \boldsymbol{\tau} \in \boldsymbol{\mathcal{Z}} : \int_I (\boldsymbol{\tau}, \boldsymbol{\varepsilon}(\dot{\mathbf{w}})) \, \mathrm{d}t = L(\mathbf{w}) - \int_I (\rho \ddot{\hat{\mathbf{u}}}, \dot{\mathbf{w}}) \, \mathrm{d}t \quad \forall \mathbf{w} \in \boldsymbol{\mathcal{W}} \right\}, \tag{17}$$

where

$$\boldsymbol{\mathcal{Z}} := \left\{ \boldsymbol{\tau} : \quad [\boldsymbol{\tau}]_{ij} \in L^2(\Omega \times I) \quad i, j \leq d \right\}, \tag{18}$$

and for $\boldsymbol{\tau}, \boldsymbol{\varepsilon} \in \boldsymbol{\mathcal{Z}}$

$$(\boldsymbol{\tau}, \boldsymbol{\varepsilon}) := \int_\Omega \boldsymbol{\tau} : \boldsymbol{\varepsilon} \, \mathrm{d}\Omega.$$

The space $\boldsymbol{\mathcal{S}}(\hat{\mathbf{u}})$ contains the *dynamically admissible* or *D-admissible* stresses. These stress tensors are in dynamic equilibrium with respect the external loads and with the inertia forces related to the admissible acceleration $\ddot{\hat{\mathbf{u}}}$. They can be discontinuous between mesh elements but the vector $\hat{\boldsymbol{\sigma}} \cdot \mathbf{n}$ has to be continuous across element edges. The equivalent strong condition for a function $\hat{\boldsymbol{\sigma}} \in \boldsymbol{\mathcal{S}}(\hat{\mathbf{u}})$ associated with a domain decomposition given by a finite element mesh is

$$\begin{aligned} -\nabla \cdot \hat{\boldsymbol{\sigma}} &= \mathbf{f} - \rho \ddot{\hat{\mathbf{u}}} \quad \text{on } \Omega_{\text{int}} \times I, \\ \hat{\boldsymbol{\sigma}} \cdot \mathbf{n} &= \mathbf{g} \quad \text{on } \Gamma_{\text{N}} \times I, \\ [\![\hat{\boldsymbol{\sigma}} \cdot \mathbf{n}]\!] &= \mathbf{0} \quad \text{on } \Gamma_{\text{int}} \times I, \end{aligned}$$

where Ω_{int} is the interior of the elements of the mesh and Γ_{int} is the set of all interior element edges. Note that the definition of $\boldsymbol{\mathcal{S}}(\hat{\mathbf{u}})$ requires the previous selection of a field $\hat{\mathbf{u}} \in \boldsymbol{\mathcal{U}}$. This is a particularity of the dynamic case. A method to build a D-admissible field $\hat{\boldsymbol{\sigma}}$ from the numerical solution $\hat{\mathbf{u}}$ is shown in section 3.6.

In the following, it is usefull to introduce the notations

$$\hat{\boldsymbol{\sigma}}^{\text{E}} := \mathbf{s}^{\text{E}}(\hat{\mathbf{u}}), \tag{19a}$$

$$\hat{\boldsymbol{\sigma}}^{\nu} := \hat{\boldsymbol{\sigma}} - \hat{\boldsymbol{\sigma}}^{\text{E}}, \tag{19b}$$

which are a decomposition of the admissible stress $\hat{\boldsymbol{\sigma}}$ into elastic and viscous parts, i.e. $\hat{\boldsymbol{\sigma}} = \hat{\boldsymbol{\sigma}}^{\text{E}} + \hat{\boldsymbol{\sigma}}^{\nu}$.

3.4. Global error representation and computable error bounds

The admissible pair $(\hat{\boldsymbol{\sigma}}, \hat{\mathbf{u}}) \in \boldsymbol{\mathcal{S}}(\hat{\mathbf{u}}) \times \boldsymbol{\mathcal{U}}$ defines the following error in stresses

$$\hat{\boldsymbol{\sigma}}^{\mathrm{e}} := \hat{\boldsymbol{\sigma}} - \mathbf{s}(\hat{\mathbf{u}}). \tag{20}$$

This error corresponds to the non verification of the constitutive relation (2) associated with the admissible pair. The value $\|\hat{\boldsymbol{\sigma}}^{\mathrm{e}}\|_{\sigma}$ is the so called *constitutive relation error* (following the terminology by Ladevèze and co-workers) and it is computable once the fields $\hat{\boldsymbol{\sigma}}$ and $\hat{\mathbf{u}}$ available. Note that, $\|\hat{\boldsymbol{\sigma}}^{\mathrm{e}}\|_{\sigma} = 0$ if and only if $\hat{\boldsymbol{\sigma}} = \boldsymbol{\sigma}$ and $\hat{\mathbf{u}} = \mathbf{u}$. Consequently, $\|\hat{\boldsymbol{\sigma}}^{\mathrm{e}}\|_{\sigma}$ is adopted as a pertinent error measure. Moreover, the value $\|\hat{\boldsymbol{\sigma}}^{\mathrm{e}}\|_{\sigma}$ is also meaningful because it is related with the unknown error $\hat{\mathbf{e}}$.

Theorem 1. *Given an admissible pair* $(\hat{\boldsymbol{\sigma}}, \hat{\mathbf{u}}) \in \boldsymbol{\mathcal{S}}(\hat{\mathbf{u}}) \times \boldsymbol{\mathcal{U}}$*, the errors defined in equations* (20) *and* (11)*,* $\hat{\boldsymbol{\sigma}}^{\mathrm{e}}$ *and* $\hat{\mathbf{e}}$*, fulfill*

$$\|\hat{\boldsymbol{\sigma}}^{\mathrm{e}}\|_{\sigma}^2 = |\dot{\hat{\mathbf{e}}}|_{t=T}^2 + \|\hat{\mathbf{e}}\|_{t=T}^2 + \|\hat{\mathbf{e}}\|^2 + \|\boldsymbol{\sigma}^{\nu} - \hat{\boldsymbol{\sigma}}^{\nu}\|_{\sigma}^2. \tag{21}$$

being $\boldsymbol{\sigma}^{\nu}$ *and* $\hat{\boldsymbol{\sigma}}^{\nu}$ *defined in* (4b) *and* (19b)*.*

Proof. First, note that $\|\hat{\boldsymbol{\sigma}}^{\mathrm{e}}\|_{\sigma}^2$ can be rewritten as

$$\|\hat{\boldsymbol{\sigma}}^{\mathrm{e}}\|_{\sigma}^2 = \|\hat{\boldsymbol{\sigma}} - \mathbf{s}(\hat{\mathbf{u}})\|_{\sigma}^2 = \|\hat{\boldsymbol{\sigma}}^{\nu} - \mathbf{s}^{\nu}(\hat{\mathbf{u}})\|_{\sigma}^2.$$

Adding and subtracting $\boldsymbol{\sigma}^{\nu}$ in the last term yields

$$\begin{aligned}\|\hat{\boldsymbol{\sigma}}^{\mathrm{e}}\|_{\sigma}^2 &= \|\hat{\boldsymbol{\sigma}}^{\nu} - \boldsymbol{\sigma}^{\nu} + \boldsymbol{\sigma}^{\nu} - \mathbf{s}^{\nu}(\hat{\mathbf{u}})\|_{\sigma}^2 \\ &= \|\hat{\boldsymbol{\sigma}}^{\nu} - \boldsymbol{\sigma}^{\nu}\|_{\sigma}^2 + \|\hat{\mathbf{e}}\|^2 - 2\bar{B}^{\nu}(\boldsymbol{\sigma}^{\nu} - \hat{\boldsymbol{\sigma}}^{\nu}, \boldsymbol{\sigma}^{\nu} - \mathbf{s}^{\nu}(\hat{\mathbf{u}})).\end{aligned}$$

Hence, it remains to prove that

$$\bar{B}^{\nu}(\boldsymbol{\sigma}^{\nu} - \hat{\boldsymbol{\sigma}}^{\nu}, \boldsymbol{\sigma}^{\nu} - \mathbf{s}^{\nu}(\hat{\mathbf{u}})) = -\frac{1}{2}|\dot{\hat{\mathbf{e}}}|_{t=T}^2 - \frac{1}{2}\|\hat{\mathbf{e}}\|_{t=T}^2. \tag{22}$$

By admissibility of $\hat{\mathbf{u}} \in \boldsymbol{\mathcal{U}}$ and $\hat{\boldsymbol{\sigma}} \in \boldsymbol{\mathcal{S}}(\hat{\mathbf{u}})$ it follows that

$$0 = \int_I (\rho(\ddot{\mathbf{u}} - \ddot{\hat{\mathbf{u}}}), \dot{\hat{\mathbf{e}}})\ \mathrm{d}t + \int_I (\boldsymbol{\sigma} - \hat{\boldsymbol{\sigma}}, \boldsymbol{\varepsilon}(\dot{\hat{\mathbf{e}}}))\ \mathrm{d}t. \tag{23}$$

Then, injecting the expression

$$\boldsymbol{\sigma} - \hat{\boldsymbol{\sigma}} = \mathbf{s}^{\mathrm{E}}(\mathbf{u} - \hat{\mathbf{u}}) + \boldsymbol{\sigma}^{\nu} - \hat{\boldsymbol{\sigma}}^{\nu},$$

into equation (23) one has

$$
\begin{aligned}
0 &= \int_I (\rho\ddot{\hat{\mathbf{e}}}, \dot{\hat{\mathbf{e}}})\ \mathrm{d}t + \int_I a(\hat{\mathbf{e}}, \dot{\hat{\mathbf{e}}})\ \mathrm{d}t + \bar{B}^\nu(\boldsymbol{\sigma}^\nu - \hat{\boldsymbol{\sigma}}^\nu, \boldsymbol{\sigma}^\nu - \mathbf{s}^\nu(\hat{\mathbf{u}})) \\
&= \frac{1}{2}\int_I \frac{\mathrm{d}}{\mathrm{d}t}(\rho\dot{\hat{\mathbf{e}}}, \dot{\hat{\mathbf{e}}})\ \mathrm{d}t + \frac{1}{2}\int_I \frac{\mathrm{d}}{\mathrm{d}t} a(\hat{\mathbf{e}}, \hat{\mathbf{e}})\ \mathrm{d}t + \bar{B}^\nu(\boldsymbol{\sigma}^\nu - \hat{\boldsymbol{\sigma}}^\nu, \boldsymbol{\sigma}^\nu - \mathbf{s}^\nu(\hat{\mathbf{u}})) \\
&= \frac{1}{2}\left[|\dot{\hat{\mathbf{e}}}|^2 + \|\hat{\mathbf{e}}\|^2\right]_{t=0}^{t=T} + \bar{B}^\nu(\boldsymbol{\sigma}^\nu - \hat{\boldsymbol{\sigma}}^\nu, \boldsymbol{\sigma}^\nu - \mathbf{s}^\nu(\hat{\mathbf{u}})).
\end{aligned}
$$

The proof is concluded by taking into account that $\hat{\mathbf{e}}(0) = \dot{\hat{\mathbf{e}}}(0) = \mathbf{0}$. □

Theorem 1 furnishes the relation $\|\hat{\boldsymbol{\sigma}}^{\mathrm{e}}\|_\sigma^2 \geq |\dot{\hat{\mathbf{e}}}|_{t=T}^2 + \|\hat{\mathbf{e}}\|_{t=T}^2 + \|\hat{\mathbf{e}}\|^2$ and, in particular, the following upper bound

$$
\|\hat{\boldsymbol{\sigma}}^{\mathrm{e}}\|_\sigma \geq \|\hat{\mathbf{e}}\|. \tag{24}
$$

Expression (24) is particularly important because it is used to bound the quantity of interest.

3.5. Construction of K-admissible fields

The firs step to build an admissible pair $(\hat{\boldsymbol{\sigma}}, \hat{\mathbf{u}}) \in \boldsymbol{\mathcal{S}}(\hat{\mathbf{u}}) \times \boldsymbol{\mathcal{U}}$ is to define the K-admissible field $\hat{\mathbf{u}} \in \boldsymbol{\mathcal{U}}$. The method of the linear accelerations [26, Ch. 7] is considered in the present case. This method is preferred because it simplifies the subsequent construction of the D-admissible field.

The basic idea is to take the admissible acceleration equal to $\mathbf{a}^{H,\Delta t}$ as defined in (9c) and then integrate in time to obtain the admissible velocity and the admissible displacement:

$$
\ddot{\hat{\mathbf{u}}}(\mathbf{x}, t) := \mathbf{a}^{H,\Delta t}(\mathbf{x}, t), \tag{25a}
$$

$$
\dot{\hat{\mathbf{u}}}(\mathbf{x}, t) := \int_0^t \ddot{\hat{\mathbf{u}}}^{H,\Delta t}(\mathbf{x}, \xi)\ \mathrm{d}\xi + \mathbf{v}_0^{H,\Delta t}(\mathbf{x}), \tag{25b}
$$

$$
\hat{\mathbf{u}}(\mathbf{x}, t) := \int_0^t \dot{\hat{\mathbf{u}}}^{H,\Delta t}(\mathbf{x}, \xi)\ \mathrm{d}\xi + \mathbf{u}_0^{H,\Delta t}(\mathbf{x}). \tag{25c}
$$

Remark 4. *The error representation presented in section 3.4 (and also its counterpart for error in quantities of inters presented in section 4.3) holds for any admissible solution $\hat{\mathbf{u}} \in \boldsymbol{\mathcal{U}}$. Note however that the stress equilibration procedures required to obtain computable bounds, see section 3.6, may require additional constrains on $\hat{\mathbf{u}} \in \boldsymbol{\mathcal{U}}$. Note that the choice for $\hat{\mathbf{u}}$ defined in equation* (25) *fulfills the requirements of the stress equilibration technique used in section 3.7.*

3.6. Construction of D-admissible fields

Once the field $\hat{\mathbf{u}} \in \boldsymbol{\mathcal{U}}$ is available, the D-admissible field is built such that $\hat{\boldsymbol{\sigma}} \in \boldsymbol{\mathcal{S}}(\hat{\mathbf{u}})$. The construction of $\hat{\boldsymbol{\sigma}}$ is more involved than the one for $\hat{\mathbf{u}}$. The reason is that the admissible stress has to be equilibrated in a dynamic sense. The dynamic equilibration reduces to static equilibration at each time $t \in \mathcal{T}$ if certain conditions are satisfied. This property allows using the standard equilibration techniques for the static problem that are well studied in the literature [26, 27, 22]. These conditions are not a strong restriction but they are worth to be stressed out. They read:

- The external loads $\mathbf{f}$ and $\mathbf{g}$ have to be continuous in time and with linear time-dependence in the time slabs of the time partition $\mathcal{T}$.
- The acceleration $\ddot{\hat{\mathbf{u}}}$ associated with the K-admissible field has to be continuous in time and with linear time-dependence in the time slabs of the timepartition $\mathcal{T}$.

Moreover, if local stress equilibration techniques [26, 27, 22] are used to compute the D-admissible field $\hat{\boldsymbol{\sigma}}$ (as in this article) further considerations should be regarded:

- The input of the local stress equilibration is not only the admissible field $\hat{\mathbf{u}}$, but also the fields $\mathbf{u}_n^{H,\Delta t}, \mathbf{v}_n^{H,\Delta t}, \mathbf{a}_n^{H,\Delta t} \in \boldsymbol{\mathcal{V}}_0^H$ fulfilling equation (8). Moreover, $\hat{\mathbf{u}}$ has to be such that $\ddot{\hat{\mathbf{u}}}(t_n) = \mathbf{a}_n^{H,\Delta t}$ for $n = 0, \cdots, N$, in order to build a stress field $\hat{\boldsymbol{\sigma}}$ fulfilling equation (18). In a practical point of view, it means that the fields $\mathbf{u}_n^{H,\Delta t}, \mathbf{v}_n^{H,\Delta t}, \mathbf{a}_n^{H,\Delta t}$ cannot be cleared out once the field $\hat{\mathbf{u}}$ is available.

The following theorem demonstrates how the dynamic equilibration reduces to a bunch of static equilibrations.

Theorem 2. *Given the external loads $\mathbf{f}, \mathbf{g}$ and a K-admissible field $\hat{\mathbf{u}} \in \boldsymbol{\mathcal{U}}$, then a D-admissible stress $\hat{\boldsymbol{\sigma}} \in \boldsymbol{\mathcal{S}}(\hat{\mathbf{u}})$ is straightforwardly defined through linear interpolation in time*

$$\hat{\boldsymbol{\sigma}}(\mathbf{x}, t) := \sum_{n=0}^{N} \hat{\boldsymbol{\sigma}}_n(\mathbf{x}) \theta_n(t), \tag{26}$$

provided that: 1) the stress fields $\hat{\boldsymbol{\sigma}}_n,\ n = 0, \ldots, N$ fulfill the static equilibrium condition

$$(\hat{\boldsymbol{\sigma}}_n, \boldsymbol{\varepsilon}(\mathbf{w})) = l_n(\mathbf{w}) - (\rho \ddot{\hat{\mathbf{u}}}_n, \mathbf{w}) \quad \forall \mathbf{w} \in \boldsymbol{\mathcal{V}}_0, \tag{27}$$

and 2) the external loads $\mathbf{f}, \mathbf{g}$ *and the acceleration* $\ddot{\hat{\mathbf{u}}}$ *are piecewise linear in time, i.e.*

$$\mathbf{f}(\mathbf{x}, t) = \sum_{n=0}^{N} \mathbf{f}_n(\mathbf{x})\theta_n(t), \tag{28a}$$

$$\mathbf{g}(\mathbf{x}, t) = \sum_{n=0}^{N} \mathbf{g}_n(\mathbf{x})\theta_n(t), \tag{28b}$$

$$\ddot{\hat{\mathbf{u}}}(\mathbf{x}, t) = \sum_{n=0}^{N} \ddot{\hat{\mathbf{u}}}_n(\mathbf{x})\theta_n(t). \tag{28c}$$

Proof. The proof is obtained introducing expressions (28) and (26) in the definition (17). □

Theorem 2 allows building the admissible field $\hat{\boldsymbol{\sigma}}$ from the stresses $\hat{\boldsymbol{\sigma}}_n,\ n = 0, \cdots, N$ fulfilling equation (27). The stress fields $\hat{\boldsymbol{\sigma}}_n$ are not unique and they can be computed with different techniques, e.g. [26, 28].

References [26, 28] deal with strict estimates. That is, they provide stress fields $\hat{\boldsymbol{\sigma}}_n$ fulfilling exactly equation (27). This work focuses in asymptotic estimates, i.e. equations (27) are solved using a reference mesh. The resulting approximations to stresses $\hat{\boldsymbol{\sigma}}_n$ fulfill equations (27) only asymptotically, that is the equilibrium condition is fulfilled if the element size of the reference mesh tends to zero. The asymptotic approach is adopted for its ease of implementation. However, it is worth noting that all the developments (except the remainder of this section) are general and also valid for strict estimates.

A direct version (but prohibitive) of an asymptotic estimate is to approximate $\hat{\boldsymbol{\sigma}}_n$ with a displacement-based problem using a global reference mesh with element size $h \ll H$. This mesh can be generated as a nested subdivision of the existing one, generating the space $\boldsymbol{\mathcal{V}}_0^h$ such that $\boldsymbol{\mathcal{V}}_0^H \subset \boldsymbol{\mathcal{V}}_0^h \subset \boldsymbol{\mathcal{V}}_0$. The reference problem providing this solution reads: find $\mathbf{u}^h \in \boldsymbol{\mathcal{V}}_0^h$ such that

$$a(\mathbf{u}_n^h, \mathbf{w}) = l_n(\mathbf{w}) - (\rho\ddot{\hat{\mathbf{u}}}_n, \mathbf{w}) \quad \forall \mathbf{w} \in \boldsymbol{\mathcal{V}}_0^h.$$

The displacement field $\mathbf{u}_n^h$ is associated with the stress field $\hat{\boldsymbol{\sigma}}_n^{\text{ref}} := \boldsymbol{\mathcal{C}} : \boldsymbol{\varepsilon}(\mathbf{u}^h)$. The time dependent stress $\hat{\boldsymbol{\sigma}}^{\text{ref}}$ is defined from all the $\hat{\boldsymbol{\sigma}}_n^{\text{ref}}$ in the same fashion as for equation (26):

$$\hat{\boldsymbol{\sigma}}^{\text{ref}}(\mathbf{x}, t) := \sum_{n=0}^{N} \theta_n(t)\hat{\boldsymbol{\sigma}}_n^{\text{ref}}(\mathbf{x}). \tag{29}$$

In the remainder of the paper, for all practical purposes, $\hat{\boldsymbol{\sigma}}^{\text{ref}}$ is assumed to fairly replace $\hat{\boldsymbol{\sigma}}$ as for the results concerning the error in the constitutive relation introduced in section 3.4.

3.7. Flux-free error estimates

The methods allowing to compute a D-admissible stress field with an affordable computational cost require using domain decomposition. That is, solving local counterparts of equations (27). The two main approaches for domain decomposition are the hybrid-flux [26] and the flux-free methodologies [22], using respectively as local subdomains the elements and patches of elements centered in one node (stars). Other approaches furnish D-admissible fields solving global dual problems (having stresses as unknowns) on the original finite element mesh, see for instance [29, 30]. Here, the flux-free approach is selected.

This section is devoted to briefly review this technique and its specific application in the context of this paper. The objective is generating a collection of stress fields $\hat{\boldsymbol{\sigma}}_n^{\mathrm{ff}}$ fulfilling an asymptotic version of equations (27). Thus, an asymptotically D-admissible stress $\hat{\boldsymbol{\sigma}}^{\mathrm{ff}}$ is computed from $\hat{\boldsymbol{\sigma}}_n^{\mathrm{ff}}$ similarly to (29).

The stress fields $\hat{\boldsymbol{\sigma}}_n^{\mathrm{ff}}$, $n = 0, \ldots, N$, are generated using approximations to the error in displacements at time t_n, $\tilde{\mathbf{e}}_n$, namely

$$\hat{\boldsymbol{\sigma}}_n^{\mathrm{ff}} := \boldsymbol{\mathcal{C}} : \boldsymbol{\varepsilon}(\tilde{\mathbf{e}}_n + \mathbf{u}_n^{H,\Delta t} + \tau \mathbf{v}_n^{H,\Delta t}). \tag{30}$$

As previously said, the estimates $\tilde{\mathbf{e}}_n$ are obtained with the flux free method, see [22] for details, as a sum of local contributions associated with patches of elements. The main rationale of this method is to compute function $\tilde{\mathbf{e}}_n$ as the addition of local estimates $\tilde{\mathbf{e}}_n^i$, i.e.

$$\tilde{\mathbf{e}}_n := \sum_{i \in \mathcal{N}} \tilde{\mathbf{e}}_n^i, \tag{31}$$

where $\mathcal{N}$ is the set of the indices of the vertex nodes in the mesh. In fact, each local estimate $\tilde{\mathbf{e}}_n^i$ is computed in the element patch centered at the i-th node, $i \in \mathcal{N}$. This element patch is defined as the support of the shape function ϕ^i of the i-th node, that is $\omega^i := \mathrm{supp}(\phi^i)$.

The local estimate $\tilde{\mathbf{e}}_n^i$ lives in the space $\boldsymbol{\mathcal{V}}_{\omega^i}^h$ which is the restriction of $\boldsymbol{\mathcal{V}}_0^h$ to ω^i, namely

$$\boldsymbol{\mathcal{V}}_{\omega^i}^h := \boldsymbol{\mathcal{V}}_0^h \cap [H^1(\omega^i)]^d.$$

The sum of all these local spaces generates the broken space $\widehat{\boldsymbol{\mathcal{V}}}_0^h$ which is the space where $\tilde{\mathbf{e}}_n$ lives. Functions in $\widehat{\boldsymbol{\mathcal{V}}}_0^h$ are of the same type as in $\boldsymbol{\mathcal{V}}_0^h$ but they are allowed to be discontinuous between the elements of the mesh.

Each local estimate $\tilde{\mathbf{e}}_n^i$ is one solution of the problem: find $\tilde{\mathbf{e}}_n^i \in \boldsymbol{\mathcal{V}}_{\omega^i}^h$ such that

$$a(\tilde{\mathbf{e}}_n^i, \mathbf{w}) = R_n(\phi^i(\mathbf{w} - \boldsymbol{\Pi}^H \mathbf{w})) \quad \forall \mathbf{w} \in \boldsymbol{\mathcal{V}}_{\omega^i}^h, \tag{32}$$

where

$$R_n(\mathbf{w}) := l_n(\mathbf{w}) - (\rho \mathbf{a}_n^{H,\Delta t}, \mathbf{w}) - a(\mathbf{u}_n^{H,\Delta t} + \tau \mathbf{v}^{H,\Delta t}, \mathbf{w}), \tag{33}$$

is the residual of the Newmark solution at time $t_n \in \mathcal{T}$. The operator $\mathbf{\Pi}^H : \boldsymbol{\mathcal{V}}_0 \to \boldsymbol{\mathcal{V}}_0^H$ is the interpolation operator in $\boldsymbol{\mathcal{V}}_0^H$.

It is worth noting that the flux-free method (or other alternative local stress equilibration technique) requires that the residual R_n fulfills Galerkin orthogonality. It is crucial in the well-posedness (solvability) of the local problems. In fact, for the residual R_n introduced in (33), the following expression holds

$$R_n(\mathbf{w}) = 0 \quad \forall \mathbf{w} \in \boldsymbol{\mathcal{V}}_0^H.$$

Recall that the definition of the D-admissible space $\boldsymbol{\mathcal{S}}(\hat{\mathbf{u}})$ depends on $\hat{\mathbf{u}}$. Note however that $\hat{\mathbf{u}}$ is not explicitly involved in equation (32), which is the seed problem to provide $\hat{\boldsymbol{\sigma}}^{\mathrm{ff}}$. This is not contradictory because the K-admissible field $\hat{\mathbf{u}}$ is build such that $\ddot{\hat{\mathbf{u}}} = \mathbf{a}^{H,\Delta t}$.

Once $\tilde{\mathbf{e}}_n^i$ are computed for $i \in \mathcal{N}$ solving (32), $\tilde{\mathbf{e}}_n$ is recovered using (31) and the stress field $\hat{\boldsymbol{\sigma}}_n^{\mathrm{ff}}$ follows from (30). The D-admissible estimate $\hat{\boldsymbol{\sigma}}^{\mathrm{ff}}$ is completed using the time interpolation analogous to (29).

The flux-free recovered stresses $\hat{\boldsymbol{\sigma}}^{\mathrm{ff}}$ is D-admissible in the asymptotic sense, that is fulfilling equilibrium as stated is equation (17) but referred to a discrete space associated with the reference h-mesh (replacing $\boldsymbol{\mathcal{W}}$ by the discrete h-version). Thus, the estimate provided by $\hat{\boldsymbol{\sigma}}^{\mathrm{ff}}$ does not yield a strict upper bound with respect to the exact error, as indicated in theorem 1. Nevertheless, the flux-free estimate furnishes an asymptotic upper bound, that is a true upper bound with respect to the reference quantity associated with $\hat{\boldsymbol{\sigma}}^{\mathrm{ref}}$. This is stated in the following theorem.

Theorem 3. *Given the K-admissible field $\hat{\mathbf{u}} \in \boldsymbol{\mathcal{U}}$ defined in* (25)*, the following relation holds for the two asymptotic D-admissible fields $\hat{\boldsymbol{\sigma}}^{\mathrm{ref}}$ and $\hat{\boldsymbol{\sigma}}^{\mathrm{ff}}$*

$$\|\hat{\boldsymbol{\sigma}}^{\mathrm{ff}} - \mathbf{s}(\hat{\mathbf{u}})\|_\sigma \geq \|\hat{\boldsymbol{\sigma}}^{\mathrm{ref}} - \mathbf{s}(\hat{\mathbf{u}})\|_\sigma. \tag{34}$$

Proof. Note that $\hat{\boldsymbol{\sigma}}^{\mathrm{ff}}$ and $\hat{\boldsymbol{\sigma}}^{\mathrm{ref}}$ can be expressed as

$$\hat{\boldsymbol{\sigma}}^{\mathrm{ref}} = \boldsymbol{\mathcal{C}} : \boldsymbol{\varepsilon}(\mathbf{u}^{H,\Delta t} + \tau \mathbf{v}^{H,\Delta t} + \mathbf{e}^h),$$
$$\hat{\boldsymbol{\sigma}}^{\mathrm{ff}} = \boldsymbol{\mathcal{C}} : \boldsymbol{\varepsilon}(\mathbf{u}^{H,\Delta t} + \tau \mathbf{v}^{H,\Delta t} + \tilde{\mathbf{e}}).$$

by considering

$$\mathbf{u}^h(\mathbf{x},t) := \sum_{n=0}^{N} \mathbf{u}_n^h(\mathbf{x})\theta_n(t), \quad \tilde{\mathbf{e}}(\mathbf{x},t) := \sum_{n=0}^{N} \tilde{\mathbf{e}}_n(\mathbf{x})\theta_n(t) \quad \text{and} \quad \mathbf{e}^h := \mathbf{u}^h - \mathbf{u}^{H,\Delta t} - \tau \mathbf{v}^{H,\Delta t}.$$

Thus,

$$\begin{aligned}\|\hat{\boldsymbol{\sigma}}^{\mathrm{ref}} - \mathbf{s}(\hat{\mathbf{u}})\|_\sigma^2 &= \frac{1}{\tau}\int_I \|\mathbf{e}^h + (\mathbf{u}^{H,\Delta t} - \hat{\mathbf{u}}) + \tau(\mathbf{v}^{H,\Delta t} - \dot{\hat{\mathbf{u}}})\|^2 \ \ \mathrm{d}t \\ &= \frac{1}{\tau}\int_I \left\{\|\mathbf{e}^h\|^2 + \|\mathbf{s}\|^2 + 2a(\mathbf{e}^h, \mathbf{s})\right\} \ \ \mathrm{d}t,\end{aligned}$$

and

$$\begin{aligned}\|\hat{\boldsymbol{\sigma}}^{\mathrm{ff}} - \mathbf{s}(\hat{\mathbf{u}})\|_\sigma^2 &= \frac{1}{\tau}\int_I \|\tilde{\mathbf{e}} + (\mathbf{u}^{H,\Delta t} - \hat{\mathbf{u}}) + \tau(\mathbf{v}^{H,\Delta t} - \dot{\hat{\mathbf{u}}})\|^2 \ \ \mathrm{d}t \\ &= \frac{1}{\tau}\int_I \left\{\|\tilde{\mathbf{e}}\|^2 + \|\mathbf{s}\|^2 + 2a(\tilde{\mathbf{e}}, \mathbf{s})\right\} \ \ \mathrm{d}t,\end{aligned} \tag{35}$$

where

$$\mathbf{s} := (\mathbf{u}^{H,\Delta t} - \hat{\mathbf{u}}) + \tau(\mathbf{v}^{H,\Delta t} - \dot{\hat{\mathbf{u}}}).$$

Then, the proof of the theorem reduces to

$$\|\tilde{\mathbf{e}}\|^2 + 2a(\tilde{\mathbf{e}}, \mathbf{s}) \geq \|\mathbf{e}^h\|^2 + 2a(\mathbf{e}^h, \mathbf{s}).$$

Note that fields $\mathbf{e}^h$ and $\tilde{\mathbf{e}}$ have been defined such that

$$R(\mathbf{s}) = a(\tilde{\mathbf{e}}, \mathbf{s}) = a(\mathbf{e}^h, \mathbf{s}),$$

where

$$R(\mathbf{w}(\mathbf{x}, t)) := \sum_{n=0}^{N} R_n(\mathbf{w}(\mathbf{x}, t_n))\theta_n(t).$$

The proof is concluded by observing that

$$\|\tilde{\mathbf{e}}\|^2 \geq \|\mathbf{e}^h\|^2,$$

which is a consequence of the construction of the flux-free estimates, see [22] for details. □

4. Bounds of linear functional outputs

4.1. Quantity of interest

The present study aims at obtaining bounds for some given quantity of interest of the solution, denoted by $L^{\mathcal{O}}(\mathbf{u})$, being $L^{\mathcal{O}}$ a linear form such that

$$\begin{aligned} L^{\mathcal{O}} : \boldsymbol{\mathcal{U}} &\longrightarrow \mathbb{R} \\ \mathbf{w} &\longmapsto L^{\mathcal{O}}(\mathbf{w}). \end{aligned}$$

The structure of $L^{\mathcal{O}}$ is restricted to be as follows:

$$\begin{aligned} L^{\mathcal{O}}(\mathbf{w}) := & \int_I (\mathbf{f}^{\mathcal{O}}, \dot{\mathbf{w}}) \, \mathrm{d}t && \text{(average of velocities in } \Omega \times I) \\ & + \int_I (\mathbf{g}^{\mathcal{O}}, \dot{\mathbf{w}})_{\Gamma_{\mathrm{N}}} \, \mathrm{d}t && \text{(average of velocities on } \Gamma_{\mathrm{N}} \times I) \\ & + (\rho \mathbf{v}^{\mathcal{O}}, \dot{\mathbf{w}}(T)) && \text{(average of velocities at } \Omega \times \{T\}) \\ & + a(\mathbf{u}^{\mathcal{O}}, \mathbf{w}(T)) && \text{(average of strains at } \Omega \times \{T\}), \end{aligned} \tag{36}$$

where $\mathbf{f}^{\mathcal{O}}$, $\mathbf{g}^{\mathcal{O}}$, $\mathbf{v}^{\mathcal{O}}$ and $\mathbf{u}^{\mathcal{O}}$ are the data characterizing the quantity of interest. The interpretation of each term of the previous equation is indicated inline, being $\mathbf{w}$ a displacement. This functional is rewritten in a more compact form:

$$L^{\mathcal{O}}(\mathbf{w}) = L^{\mathrm{d}}(\mathbf{w}) + (\rho \mathbf{v}^{\mathcal{O}}, \dot{\mathbf{w}}(T)) + a(\mathbf{u}^{\mathcal{O}}, \mathbf{w}(T)), \tag{37}$$

where

$$\begin{aligned} L^{\mathrm{d}}(\mathbf{w}) &:= \int_I l^{\mathrm{d}}(\dot{\mathbf{w}}) \, \mathrm{d}t, \\ l^{\mathrm{d}}(\mathbf{v}) &:= (\mathbf{f}^{\mathcal{O}}, \mathbf{w}) + (\mathbf{g}^{\mathcal{O}}, \mathbf{w})_{\Gamma_{\mathrm{N}}}. \end{aligned}$$

4.2. Adjoint problem

The *adjoint* or *dual* problem of equations (1) associated with the quantity of interest given in (36) consists in finding $\mathbf{u}^{\mathrm{d}}$ such that

$$\rho \ddot{\mathbf{u}}^{\mathrm{d}} - \boldsymbol{\nabla} \cdot \boldsymbol{\sigma}^{\mathrm{d}} = \mathbf{f}^{\mathcal{O}} \quad \text{in } \Omega \times I, \tag{38a}$$

$$\mathbf{u}^{\mathrm{d}} = \mathbf{0} \quad \text{on } \Gamma_{\mathrm{D}} \times I, \tag{38b}$$

$$\boldsymbol{\sigma}^{\mathrm{d}} \cdot \mathbf{n} = \mathbf{g}^{\mathcal{O}} \quad \text{on } \Gamma_{\mathrm{N}} \times I, \tag{38c}$$

$$\mathbf{u}^{\mathrm{d}} = -\mathbf{u}^{\mathcal{O}} \quad \text{at } \Omega \times \{T\}, \tag{38d}$$

$$\dot{\mathbf{u}}^{\mathrm{d}} = -\mathbf{v}^{\mathcal{O}} \quad \text{at } \Omega \times \{T\}, \tag{38e}$$

with the constitutive law

$$\boldsymbol{\sigma}^{\mathrm{d}} := \boldsymbol{\mathcal{C}} : \boldsymbol{\varepsilon}(\mathbf{u}^{\mathrm{d}} - \tau \dot{\mathbf{u}}^{\mathrm{d}}). \tag{39}$$

The external loads and final conditions of the adjoint problem are determined by the definition of quantity of interest in equation (36). The adjoint problem has not the same form as the original one because it has final conditions instead of initial ones and negative damping.

Remark 5. *The adjoint problem* (38) *has the same form as the original* (1) *if integrated backwards in time. Note that introducing the change of variables* $t^\star := T - t$*, the associated new unknown is*

$$\mathbf{u}^\star(t^\star) := \mathbf{u}^{\mathrm{d}}(T - t^\star),$$

which is solution of the following equations

$$\rho\ddot{\mathbf{u}}^\star - \boldsymbol{\nabla}\cdot\boldsymbol{\sigma}^\star = \mathbf{f}^{\mathcal{O}} \quad \textit{in } \Omega\times I, \tag{40a}$$

$$\mathbf{u}^\star = \mathbf{0} \quad \textit{on } \Gamma_D\times I, \tag{40b}$$

$$\boldsymbol{\sigma}^\star\cdot\mathbf{n} = \mathbf{g}^{\mathcal{O}} \quad \textit{on } \Gamma_N\times I, \tag{40c}$$

$$\mathbf{u}^\star = -\mathbf{u}^{\mathcal{O}} \quad \textit{at } \Omega\times\{t^\star = 0\}, \tag{40d}$$

$$\dot{\mathbf{u}}^\star = \mathbf{v}^{\mathcal{O}} \quad \textit{at } \Omega\times\{t^\star = 0\}, \tag{40e}$$

with

$$\boldsymbol{\sigma}^\star := \boldsymbol{\mathcal{C}} : \boldsymbol{\varepsilon}(\mathbf{u}^\star + \tau\dot{\mathbf{u}}^\star).$$

Note that problem (40) *has exactly the same form (including stability properties associated with the sign of the damping term) as* (1)*.*

A variational setting for the adjoint problem (38) is required in the following. To this end, the adjoint trial space is defined as

$$\boldsymbol{\mathcal{U}}^{\mathrm{d}} := \left\{ \mathbf{w}\in\boldsymbol{\mathcal{W}} : \begin{array}{ll} \mathbf{w} = -\mathbf{u}^{\mathcal{O}} & \text{at } \Omega\times\{T\}, \\ \dot{\mathbf{w}} = -\mathbf{v}^{\mathcal{O}} & \text{at } \Omega\times\{T\} \end{array} \right\}.$$

The set $\boldsymbol{\mathcal{U}}^{\mathrm{d}}$ contains the *adjoint kinematically admissible* or *adjoint K-admissible* displacements. These functions have the same regularity constrains and boundary conditions as the ones in $\boldsymbol{\mathcal{U}}$ and the final conditions of the adjoint problem (38).

With this notation, the weak form of the adjoint problem (38) reads: find $\mathbf{u}^{\mathrm{d}}\in\boldsymbol{\mathcal{U}}^{\mathrm{d}}$ such that

$$B^{\mathrm{d}}(\mathbf{u}^{\mathrm{d}},\mathbf{w}) = L^{\mathrm{d}}(\mathbf{w}) \quad \forall\mathbf{w}\in\boldsymbol{\mathcal{W}}, \tag{41}$$

where for $\mathbf{v},\mathbf{w}\in\boldsymbol{\mathcal{W}}$

$$B^{\mathrm{d}}(\mathbf{v},\mathbf{w}) := \int_I (\rho\ddot{\mathbf{v}},\dot{\mathbf{w}})\ \mathrm{d}t + \int_I a(\mathbf{v}-\tau\dot{\mathbf{v}},\dot{\mathbf{w}})\ \mathrm{d}t.$$

Note that B^{d} is similar to the bilinear form of the original problem defined in equation (6a) but with opposite sign of the damping term. The following relation holds between forms B and B^{d}:

$$B(\mathbf{v},\mathbf{w}) = -B^{\mathrm{d}}(\mathbf{w},\mathbf{v}) + \left[(\rho\dot{\mathbf{w}},\dot{\mathbf{v}}) + a(\mathbf{w},\mathbf{v})\right]_{t=0}^{t=T}. \tag{42}$$

This relation is easily derived noting that

$$\begin{aligned} B(\mathbf{v},\mathbf{w}) &= \int_I (\rho\ddot{\mathbf{v}},\dot{\mathbf{w}})\ \mathrm{d}t + \int_I a(\mathbf{v}+\tau\dot{\mathbf{v}},\dot{\mathbf{w}})\ \mathrm{d}t \\ &= -\int_I (\rho\ddot{\mathbf{w}},\dot{\mathbf{v}})\ \mathrm{d}t - \int_I a(\mathbf{w}-\tau\dot{\mathbf{w}},\dot{\mathbf{v}})\ \mathrm{d}t \\ &+ \left[(\rho\dot{\mathbf{w}},\dot{\mathbf{v}}) + a(\mathbf{w},\mathbf{v})\right]_{t=0}^{t=T}. \end{aligned}$$

4.3. Error representation in the quantity of interest

Bounds of the quantity of interest $L^{\mathcal{O}}(\mathbf{u})$ are obtained combining admissible pairs for both the original and the adjoint problem, $(\hat{\boldsymbol{\sigma}},\hat{\mathbf{u}})$ and $(\hat{\boldsymbol{\sigma}}^{\mathrm{d}},\hat{\mathbf{u}}^{\mathrm{d}})$. These admissible pairs allow to express the error in the quantity of interest $L^{\mathcal{O}}(\hat{\mathbf{e}})$ in terms of energy products, see theorem 4 below. Moreover, bounds for the quantity of interest are obtained from energy estimates, using equation (24) or similar variations.

The admissible pair for the adjoint problem (38) is obtained such that $(\hat{\boldsymbol{\sigma}}^{\mathrm{d}},\hat{\mathbf{u}}^{\mathrm{d}}) \in \boldsymbol{\mathcal{S}}(\hat{\mathbf{u}}^{\mathrm{d}}) \times \boldsymbol{\mathcal{U}}^{\mathrm{d}}$. The space of *adjoint dynamically admissible* or *adjoint D-admissible* fields is defined for a given $\hat{\mathbf{u}}^{\mathrm{d}} \in \boldsymbol{\mathcal{U}}^{\mathrm{d}}$ as follows

$$\boldsymbol{\mathcal{S}}^{\mathrm{d}}(\hat{\mathbf{u}}^{\mathrm{d}}) := \left\{ \boldsymbol{\tau} \in \boldsymbol{\mathcal{Z}} : \quad \int_I (\boldsymbol{\tau},\boldsymbol{\varepsilon}(\dot{\mathbf{w}}))\ \mathrm{d}t = L^{\mathrm{d}}(\mathbf{w}) - \int_I (\rho\ddot{\hat{\mathbf{u}}}^{\mathrm{d}},\dot{\mathbf{w}})\ \mathrm{d}t \quad \forall \mathbf{w} \in \boldsymbol{\mathcal{W}} \right\}.$$

The space $\boldsymbol{\mathcal{S}}^{\mathrm{d}}(\hat{\mathbf{u}}^{\mathrm{d}})$ contains stress tensors in dynamic equilibrium respect to the loads of the adjoint problem and the inertia related to the acceleration $\ddot{\hat{\mathbf{u}}}^{\mathrm{d}}$.

The admissible pair $(\hat{\boldsymbol{\sigma}}^{\mathrm{d}},\hat{\mathbf{u}}^{\mathrm{d}}) \in \boldsymbol{\mathcal{S}}(\hat{\mathbf{u}}^{\mathrm{d}}) \times \boldsymbol{\mathcal{U}}^{\mathrm{d}}$ determines the error in stresses for the adjoint problem:

$$\hat{\boldsymbol{\sigma}}^{\mathrm{d,e}} := \hat{\boldsymbol{\sigma}}^{\mathrm{d}} - \mathbf{s}^{\mathrm{E}}(\hat{\mathbf{u}}^{\mathrm{d}}) + \mathbf{s}^{\nu}(\hat{\mathbf{u}}^{\mathrm{d}}),$$

which corresponds to the non verification of the constitutive relation of the adjoint problem (39). The constitutive relation error of the adjoint problem is the value $|||\hat{\boldsymbol{\sigma}}^{\mathrm{d,e}}|||_{\sigma}$.

The errors $\hat{\boldsymbol{\sigma}}^{\mathrm{e}}$ and $\hat{\boldsymbol{\sigma}}^{\mathrm{d,e}}$ are seen as the solutions of the residual error equations

$$\bar{B}^{\nu}(\hat{\boldsymbol{\sigma}}^{\mathrm{e}},\mathbf{s}^{\nu}(\mathbf{w})) = \hat{R}(\mathbf{w}) \quad \forall \mathbf{w} \in \boldsymbol{\mathcal{W}}, \tag{43a}$$

$$\bar{B}^{\nu}(\hat{\boldsymbol{\sigma}}^{\mathrm{d,e}},\mathbf{s}^{\nu}(\mathbf{w})) = \hat{R}^{\mathrm{d}}(\mathbf{w}) \quad \forall \mathbf{w} \in \boldsymbol{\mathcal{W}}, \tag{43b}$$

where the residual for the adjoint problem is defined by

$$\hat{R}^{\mathrm{d}}(\mathbf{w}) := L^{\mathrm{d}}(\mathbf{w}) - B^{\mathrm{d}}(\hat{\mathbf{u}}^{\mathrm{d}},\mathbf{w}).$$

The previous relations are easily derived from the definition of D-admissibility. For instance, equation (43a) follows from the property included in the definition of $\boldsymbol{\mathcal{S}}(\hat{\mathbf{u}})$ in equation (17) by simply subtracting $\int_I a(\hat{\mathbf{u}} + \tau\dot{\hat{\mathbf{u}}}, \dot{\mathbf{w}})\, \mathrm{d}t$ at each hand side. The proof for (43b) is analogous.

Theorem 4. *If $(\hat{\boldsymbol{\sigma}}, \hat{\mathbf{u}}) \in \boldsymbol{\mathcal{S}}(\hat{\mathbf{u}}) \times \boldsymbol{\mathcal{U}}$ and $(\hat{\boldsymbol{\sigma}}^d, \hat{\mathbf{u}}^d) \in \boldsymbol{\mathcal{S}}^d(\hat{\mathbf{u}}^d) \times \boldsymbol{\mathcal{U}}^d$ are two admissible pairs for the original and adjoint problems, then the following error representation holds*

$$L^{\mathcal{O}}(\hat{\mathbf{e}}) + \hat{\alpha} = \hat{R}^{\mathrm{d}}(\hat{\mathbf{e}}), \tag{44}$$

or alternatively

$$L^{\mathcal{O}}(\hat{\mathbf{e}}) + \hat{\alpha} = \bar{B}^{\nu}(\hat{\boldsymbol{\sigma}}^{\mathrm{d,e}}, \mathbf{s}^{\nu}(\hat{\mathbf{e}})), \tag{45}$$

where $\hat{\alpha}$ is the following correcting term

$$\hat{\alpha} := \hat{R}(\hat{\mathbf{u}}^{\mathrm{d}}) = \bar{B}^{\nu}(\hat{\boldsymbol{\sigma}}^{\mathrm{e}}, \mathbf{s}^{\nu}(\hat{\mathbf{u}}^{\mathrm{d}})).$$

Proof. Introducing $\hat{\mathbf{e}}$ in the definition of $L^{\mathcal{O}}$ in equation (37) and using the statement of the adjoint problem (41), it yields

$$L^{\mathcal{O}}(\hat{\mathbf{e}}) = B^{\mathrm{d}}(\mathbf{u}^{\mathrm{d}}, \hat{\mathbf{e}}) + (\rho\mathbf{v}^{\mathcal{O}}, \hat{\mathbf{e}}(T)) + a(\mathbf{u}^{\mathcal{O}}, \hat{\mathbf{e}}(T)).$$

Adding and subtracting $\hat{\mathbf{u}}^{\mathrm{d}}$ in the first argument of B^{d}, it yields

$$\begin{aligned} L^{\mathcal{O}}(\hat{\mathbf{e}}) = {} & B^{\mathrm{d}}(\mathbf{u}^{\mathrm{d}} - \hat{\mathbf{u}}^{\mathrm{d}}, \hat{\mathbf{e}}) + B^{\mathrm{d}}(\hat{\mathbf{u}}^{\mathrm{d}}, \hat{\mathbf{e}}) \\ & + (\rho\mathbf{v}^{\mathcal{O}}, \hat{\mathbf{e}}(T)) + a(\mathbf{u}^{\mathcal{O}}, \hat{\mathbf{e}}(T)). \end{aligned}$$

This expression is rewritten using the relation in equation (42), taking $\mathbf{w} = \hat{\mathbf{u}}^{\mathrm{d}}$ and $\mathbf{v} = \hat{\mathbf{e}}$,

$$\begin{aligned} L^{\mathcal{O}}(\hat{\mathbf{e}}) = {} & B^{\mathrm{d}}(\mathbf{u}^{\mathrm{d}} - \hat{\mathbf{u}}^{\mathrm{d}}, \hat{\mathbf{e}}) - B(\hat{\mathbf{e}}, \hat{\mathbf{u}}^{\mathrm{d}}) \\ & + (\rho\mathbf{v}^{\mathcal{O}}, \hat{\mathbf{e}}(T)) + a(\mathbf{u}^{\mathcal{O}}, \hat{\mathbf{e}}(T)) \\ & + \left[(\rho\hat{\mathbf{u}}^{\mathrm{d}}, \hat{\mathbf{e}}) + a(\hat{\mathbf{u}}^{\mathrm{d}}, \hat{\mathbf{e}})\right]_{t=0}^{t=T}. \end{aligned}$$

Taking into account the definition of the residuals $\hat{R}$ and $\hat{R}^{\mathrm{d}}$ and the initial conditions for the original error, $\hat{\mathbf{e}}(0) = \dot{\hat{\mathbf{e}}}(0) = \mathbf{0}$ and the final conditions for the adjoint problem, $\hat{\mathbf{u}}^{\mathrm{d}}(T) = -\mathbf{u}^{\mathcal{O}}$ and $\dot{\hat{\mathbf{u}}}^{\mathrm{d}}(T) = -\mathbf{v}^{\mathcal{O}}$, the previous expression results in

$$L^{\mathcal{O}}(\hat{\mathbf{e}}) = \hat{R}^{\mathrm{d}}(\hat{\mathbf{e}}) - \hat{R}(\hat{\mathbf{u}}^{\mathrm{d}}).$$

This proves expression (44). Expression (45) is derived using the residual representation of equations (43). □

As previously said, this result relates $L^{\mathcal{O}}(\hat{\mathbf{e}})$ with the energy-like quantities $\hat{R}^{\mathrm{d}}(\hat{\mathbf{e}})$ and $\bar{B}^{\nu}(\hat{\boldsymbol{\sigma}}^{\mathrm{d,e}}, \mathbf{s}^{\nu}(\hat{\mathbf{e}}))$. Note that $\hat{\alpha}$ accounts for the lack of Galerkin orthogonality of residual $\hat{R}$ and it is computable once the admissible fields are available.

4.4. Bounds based on the Cauchy-Schwarz inequality

Bounds based on the Cauchy-Schwarz inequality are already introduced for visco-elastodynamics in reference [18]. These bounds are derived from the error representation in equation (45) along with the Cauchy-Schwarz inequality:

$$|L^{\mathcal{O}}(\hat{\mathbf{e}}) + \hat{\alpha}| \leq \|\hat{\boldsymbol{\sigma}}^{\mathrm{d,e}}\|_{\sigma} \|\mathbf{s}^{\nu}(\hat{\mathbf{e}})\|_{\sigma} = \|\hat{\boldsymbol{\sigma}}^{\mathrm{d,e}}\|_{\sigma} \|\hat{\mathbf{e}}\|. \tag{46}$$

Note that the last factor in the latter expression is not computable because involves the unknown error $\hat{\mathbf{e}}$. An upper bound estimate for this factor is the error in the constitutive relation of the original problem, see equation (24). Introducing this estimate in the previous equation a computable bound for the error in the quantity of interest is readily recovered:

$$|L^{\mathcal{O}}(\hat{\mathbf{e}}) + \hat{\alpha}| \leq \|\hat{\boldsymbol{\sigma}}^{\mathrm{d,e}}\|_{\sigma} \|\hat{\boldsymbol{\sigma}}^{\mathrm{e}}\|_{\sigma}.$$

The quantities defined as

$$\zeta_{\mathrm{U}}^{\mathrm{C\text{–}S}} := L^{\mathcal{O}}(\hat{\mathbf{u}}) + \|\hat{\boldsymbol{\sigma}}^{\mathrm{d,e}}\|_{\sigma} \|\hat{\boldsymbol{\sigma}}^{\mathrm{e}}\|_{\sigma} - \hat{\alpha},$$
$$\zeta_{\mathrm{L}}^{\mathrm{C\text{–}S}} := L^{\mathcal{O}}(\hat{\mathbf{u}}) - \|\hat{\boldsymbol{\sigma}}^{\mathrm{d,e}}\|_{\sigma} \|\hat{\boldsymbol{\sigma}}^{\mathrm{e}}\|_{\sigma} - \hat{\alpha},$$

are indeed upper and lower bounds of $L^{\mathcal{O}}(\mathbf{u})$, that is

$$\zeta_{\mathrm{L}}^{\mathrm{C\text{–}S}} \leq L^{\mathcal{O}}(\mathbf{u}) \leq \zeta_{\mathrm{U}}^{\mathrm{C\text{–}S}}. \tag{47}$$

5. Alternative error bounds

5.1. Alternative error representation and (non-computable) bounds

Alternative error bounds are often used in the literature to improve the poor quality of the bounds based on the Cauchy-Schwarz inequality. For instance, the parallelogram rule is applied in works [7, 31, 22] in the context of linear elasticity. Similar strategies based on algebraic identities are also applied to problems with non-symmetric bilinear forms as the case of the steady and transient convection-diffusion-reaction equations, see reference [21]. However, to the best knowledge of the authors, these kind of approaches have not been used in the framework of linear visco-elastodynamics.

In the following, an alternative error representation is used to derive error bounds for quantities of interest in the context of visco-elastodynamics. The derivation of the basic rationale requires introducing symmetrized equations for the original and adjoint errors. Note, however, that the actual implementation of these strategies does not require solving the auxiliary symmetrized problems because the upper bound estimates are computed

using only the admissible fields introduced above. These ideas are similar to those used in [21].

Consider the following symmetrized error equations: find $\hat{\mathbf{e}}^{\nu} \in \boldsymbol{\mathcal{U}}_0$ and $\hat{\mathbf{e}}^{\mathrm{d},\nu} \in \boldsymbol{\mathcal{U}}_0^{\mathrm{d}}$ such that

$$B^{\nu}(\hat{\mathbf{e}}^{\nu}, \mathbf{w}) = \hat{R}(\mathbf{w}) \quad \forall \mathbf{w} \in \boldsymbol{\mathcal{W}}, \tag{48a}$$

$$B^{\nu}(\hat{\mathbf{e}}^{\mathrm{d},\nu}, \mathbf{w}) = \hat{R}^{\mathrm{d}}(\mathbf{w}) \quad \forall \mathbf{w} \in \boldsymbol{\mathcal{W}}, \tag{48b}$$

where

$$B^{\nu}(\mathbf{v}, \mathbf{w}) := \tau \int_I a(\mathbf{v}, \mathbf{w}) \, \mathrm{d}t,$$

and

$$\boldsymbol{\mathcal{U}}_0^{\mathrm{d}} := \left\{ \mathbf{w} \in \boldsymbol{\mathcal{W}} : \quad \begin{array}{ll} \mathbf{w} = \mathbf{0} & \text{at } \Omega \times \{T\} \\ \dot{\mathbf{w}} = \mathbf{0} & \text{at } \Omega \times \{T\} \end{array} \right\}.$$

Equations (48) resemble the residual equation (12) for the error $\hat{\mathbf{e}}$. Note that the difference is that the bilinear form B is replaced by the symmetric one B^{ν}.

Theorem 5. *If* $\hat{\mathbf{e}}^{\nu}$ *and* $\hat{\mathbf{e}}^{\mathrm{d},\nu}$ *are solution of equations* (48a) *and* (48b) *then, for any* $\kappa \in \mathbb{R}$, $\kappa \neq 0$,

$$-\frac{1}{4}|\!|\!|\kappa\hat{\mathbf{e}}^{\nu} - \frac{1}{\kappa}\hat{\mathbf{e}}^{\mathrm{d},\nu}|\!|\!|^2 \leq L^{\mathcal{O}}(\hat{\mathbf{e}}) + \hat{\alpha} \leq \frac{1}{4}|\!|\!|\kappa\hat{\mathbf{e}}^{\nu} + \frac{1}{\kappa}\hat{\mathbf{e}}^{\mathrm{d},\nu}|\!|\!|^2. \tag{49}$$

Proof. Taking $\mathbf{w} = \kappa\hat{\mathbf{e}}$ in equations (48a) and (48b), a linear combination of them (with weights κ and $\pm 1/\kappa$) results in

$$B^{\nu}(\kappa\hat{\mathbf{e}}^{\nu} \pm \frac{1}{\kappa}\hat{\mathbf{e}}^{\mathrm{d},\nu}, \kappa\hat{\mathbf{e}}) = \kappa^2 \hat{R}(\hat{\mathbf{e}}) \pm \hat{R}^{\mathrm{d}}(\hat{\mathbf{e}}).$$

Taking $\mathbf{w} = \hat{\mathbf{e}}$ in equation (12) and using equation (16) it is obtained that

$$\hat{R}(\hat{\mathbf{e}}) \geq |\!|\!|\hat{\mathbf{e}}|\!|\!|^2.$$

Hence,

$$B^{\nu}(\kappa\hat{\mathbf{e}}^{\nu} \pm \frac{1}{\kappa}\hat{\mathbf{e}}^{\mathrm{d},\nu}, \kappa\hat{\mathbf{e}}) \geq \kappa^2 |\!|\!|\hat{\mathbf{e}}|\!|\!|^2 \pm L^{\mathcal{O}}(\hat{\mathbf{e}}) \pm \hat{\alpha}, \tag{50}$$

where the term involving the adjoint residual, $\hat{R}^{\mathrm{d}}(\hat{\mathbf{e}})$ has been replaced by $L^{\mathcal{O}}(\hat{\mathbf{e}}) + \hat{\alpha}$ using equation (44) of theorem 4.

On the other hand, one has that

$$B^\nu(\kappa\hat{\mathbf{e}}^\nu \pm \frac{1}{\kappa}\hat{\mathbf{e}}^{\mathrm{d},\nu}, \kappa\hat{\mathbf{e}}) - \kappa^2 |\!|\!| \hat{\mathbf{e}} |\!|\!|^2 \leq \frac{1}{4} |\!|\!| \kappa\hat{\mathbf{e}}^\nu \pm \frac{1}{\kappa}\hat{\mathbf{e}}^{\mathrm{d},\nu} |\!|\!|^2. \tag{51}$$

This is a direct consequence of considering the following expansion

$$\begin{aligned} 0 \leq |\!|\!| \frac{1}{2}(\kappa\hat{\mathbf{e}}^\nu \pm \frac{1}{\kappa}\hat{\mathbf{e}}^{\mathrm{d},\nu}) - \kappa\hat{\mathbf{e}} |\!|\!|^2 = \frac{1}{4} |\!|\!| \kappa\hat{\mathbf{e}}^\nu \pm \frac{1}{\kappa}\hat{\mathbf{e}}^{\mathrm{d},\nu} |\!|\!|^2 + \kappa^2 |\!|\!| \hat{\mathbf{e}} |\!|\!|^2 \\ - B^\nu(\kappa\hat{\mathbf{e}}^\nu \pm \frac{1}{\kappa}\hat{\mathbf{e}}^{\mathrm{d},\nu}, \kappa\hat{\mathbf{e}}). \end{aligned}$$

Thus, the proof is completed using equation (51) in equation (50)

$$\pm L^{\mathcal{O}}(\hat{\mathbf{e}}) \pm \hat{\alpha} \leq B^\nu(\kappa\hat{\mathbf{e}}^\nu \pm \frac{1}{\kappa}\hat{\mathbf{e}}^{\mathrm{d},\nu}, \kappa\hat{\mathbf{e}}) - \kappa^2 |\!|\!| \hat{\mathbf{e}} |\!|\!|^2 \leq \frac{1}{4} |\!|\!| \kappa\hat{\mathbf{e}}^\nu \pm \frac{1}{\kappa}\hat{\mathbf{e}}^{\mathrm{d},\nu} |\!|\!|^2. \qquad \square$$

Remark 6. *Theorem 5 gives an alternative error representation in the quantity of interest. The structure of bounds in expression* (49) *is similar (but not the same) to those obtained using the parallelogram rule in linear elasticity, where the error in the quantity of interest is also expressed in terms of energy measures of linear combinations of the original and adjoint errors. The main difference with respect the parallelogram rule is that, here lower bounds of the error are not computed.*

Equation (49) allows bounding $L^{\mathcal{O}}(\hat{\mathbf{e}})$ by computing $|\!|\!| \mathbf{z}^\pm |\!|\!|^2$, where $\mathbf{z}^\pm := \kappa\hat{\mathbf{e}}^\nu \pm \frac{1}{\kappa}\hat{\mathbf{e}}^{\mathrm{d},\nu}$. These two functions are solutions of

$$B^\nu(\mathbf{z}^\pm, \mathbf{w}) = \hat{R}^\pm(\mathbf{w}) \quad \forall \mathbf{w} \in \boldsymbol{\mathcal{W}}, \tag{52}$$

where

$$\hat{R}^\pm(\mathbf{w}) := \kappa\hat{R}(\mathbf{w}) \pm \frac{1}{\kappa}\hat{R}^{\mathrm{d}}(\mathbf{w}).$$

Functions $\mathbf{z}^\pm$ are solutions of the infinite dimensional problems (52). Therefore, the error bounds proposed in (49), corresponding to the values of $|\!|\!| \mathbf{z}^\pm |\!|\!|^2$, are not computable. In the following, computable bounds are obtained from an auxiliary field $\boldsymbol{\sigma}_{\mathbf{z}^\pm}$, in the same fashion as the energy-like bounds described in section 3.

5.2. Computable error bounds

As shown in sections 3 and 4, the standard approach to obtain a computable error bound is to find a D-admissible stress. The admissible stress associated with $\mathbf{z}^\pm$ is denoted by $\boldsymbol{\sigma}_{\mathbf{z}^\pm}$ which fulfills the stress-version of equation (52), i.e.

$$\bar{B}^\nu(\boldsymbol{\sigma}_{\mathbf{z}^\pm}, \mathbf{s}^\nu(\mathbf{w})) = \hat{R}^\pm(\mathbf{w}) \quad \forall \mathbf{w} \in \boldsymbol{\mathcal{W}}. \tag{53}$$

Comparing equation (53) and the residual representation of equations (43), one concludes that the following linear combination of $\hat{\boldsymbol{\sigma}}^{\mathrm{e}}$ and $\hat{\boldsymbol{\sigma}}^{\mathrm{d,e}}$

$$\boldsymbol{\sigma}_{\mathbf{z}^{\pm}} := \kappa\hat{\boldsymbol{\sigma}}^{\mathrm{e}} \pm \frac{1}{\kappa}\hat{\boldsymbol{\sigma}}^{\mathrm{d,e}}, \tag{54}$$

is solution of (53). The value $\|\boldsymbol{\sigma}_{\mathbf{z}^{\pm}}\|_{\sigma}$ is indeed an upper bound of $\|\mathbf{z}^{\pm}\|$ as the following theorem shows.

Theorem 6. *Being* $\mathbf{z}^{\pm}$ *and* $\boldsymbol{\sigma}_{\mathbf{z}^{\pm}}$ *solutions of equations* (52) *and* (53) *respectively, the following inequality holds*

$$\|\mathbf{z}^{\pm}\| \leq \|\boldsymbol{\sigma}_{\mathbf{z}^{\pm}}\|_{\sigma}.$$

Proof. On the one hand, one has that

$$\begin{aligned} 0 \leq \|\boldsymbol{\sigma}_{\mathbf{z}^{\pm}} - \mathbf{s}^{\nu}(\mathbf{z}^{\pm})\|_{\sigma}^{2} &= \|\boldsymbol{\sigma}_{\mathbf{z}^{\pm}}\|_{\sigma}^{2} + \|\mathbf{z}^{\pm}\|^{2} - 2\bar{B}^{\nu}(\boldsymbol{\sigma}_{\mathbf{z}^{\pm}}, \mathbf{s}^{\nu}(\mathbf{z}^{\pm})) \\ &= \|\boldsymbol{\sigma}_{\mathbf{z}^{\pm}}\|_{\sigma}^{2} + \|\mathbf{z}^{\pm}\|^{2} - 2\hat{R}^{\pm}(\mathbf{z}^{\pm}). \end{aligned} \tag{55}$$

On the other hand, taking $\mathbf{w} = \mathbf{z}^{\pm}$ in equation (52) one gets

$$\hat{R}^{\pm}(\mathbf{z}^{\pm}) = \|\mathbf{z}^{\pm}\|^{2},$$

The proof is completed by substituting the latter expression into the last term of equation (55), namely

$$0 \leq \|\boldsymbol{\sigma}_{\mathbf{z}^{\pm}}\|_{\sigma}^{2} - \|\mathbf{z}^{\pm}\|^{2}. \qquad \square$$

Thus, using expression (54) for $\boldsymbol{\sigma}_{\mathbf{z}^{\pm}}$, an upper bound of $\|\mathbf{z}^{\pm}\|^{2}$ is computed as

$$\|\kappa\hat{\boldsymbol{\sigma}}^{\mathrm{e}} \pm \frac{1}{\kappa}\hat{\boldsymbol{\sigma}}^{\mathrm{d,e}}\|_{\sigma} \geq \|\mathbf{z}^{\pm}\|. \tag{56}$$

As previously announced, expression (56) allows computing bounds for $L^{\mathcal{O}}(\hat{\mathbf{e}})$ without any use of the symmetrized error equations (48). In fact, the introduction of the symmetrized error equations is only a mathematical artifact that allows deriving an alternative bounding expression. The final bounds for $L^{\mathcal{O}}(\mathbf{u})$ are derived substituting expression (56) in equation (49):

$$\begin{aligned} \zeta_{\mathrm{U}} &:= L^{\mathcal{O}}(\hat{\mathbf{u}}) + \frac{1}{4}\|\kappa\hat{\boldsymbol{\sigma}}^{\mathrm{e}} + \frac{1}{\kappa}\hat{\boldsymbol{\sigma}}^{\mathrm{d,e}}\|_{\sigma}^{2} - \hat{\alpha}, \\ \zeta_{\mathrm{L}} &:= L^{\mathcal{O}}(\hat{\mathbf{u}}) - \frac{1}{4}\|\kappa\hat{\boldsymbol{\sigma}}^{\mathrm{e}} - \frac{1}{\kappa}\hat{\boldsymbol{\sigma}}^{\mathrm{d,e}}\|_{\sigma}^{2} - \hat{\alpha}, \end{aligned}$$

where ζ_{U} and ζ_{L} are such that

$$\zeta_{\mathrm{L}} \leq L^{\mathcal{O}}(\mathbf{u}) \leq \zeta_{\mathrm{U}}. \tag{57}$$

Note that $\hat{\boldsymbol{\sigma}}^{\mathrm{e}}$ and $\hat{\boldsymbol{\sigma}}^{\mathrm{d,e}}$ are eventually computed using asymptotic techniques, for instance the flux-free strategies. In this case, the upper bound properties (57) hold only asymptotically, that is if the size of the reference mesh is *small enough*. In practice, due to the overestimation introduced in the subsequent approximations, the estimates obtained are upper bound of the error in all the examples. The parameter κ is determined such that it minimizes $\|\kappa\hat{\boldsymbol{\sigma}}^{\mathrm{e}} \pm \frac{1}{\kappa}\hat{\boldsymbol{\sigma}}^{\mathrm{d,e}}\|_{\sigma}^2$. This is achieved by enforcing

$$\frac{\partial}{\partial\kappa}\|\kappa\hat{\boldsymbol{\sigma}}^{\mathrm{e}} \pm \frac{1}{\kappa}\hat{\boldsymbol{\sigma}}^{\mathrm{d,e}}\|_{\sigma}^2 = 0 \qquad \Rightarrow \qquad \kappa\|\hat{\boldsymbol{\sigma}}^{\mathrm{e}}\|_{\sigma}^2 - \frac{1}{\kappa^3}\|\hat{\boldsymbol{\sigma}}^{\mathrm{d,e}}\|_{\sigma}^2 = 0$$

that is to say

$$\kappa = \left(\frac{\|\hat{\boldsymbol{\sigma}}^{\mathrm{d,e}}\|_{\sigma}}{\|\hat{\boldsymbol{\sigma}}^{\mathrm{e}}\|_{\sigma}}\right)^{1/2}.$$

6. Numerical examples

The error bounds corresponding to the Cauchy-Schwarz formulation, see expressions (47), and the error bounds proposed here, see (57), are compared in two academic examples. The first is a 1D bar and the second a 2D plate.

6.1. Example 1: 1D bar

The visco-elastic bar of figure 1(a) is considered. It is clamped at the right end and loaded on the left end with the time dependent traction described in figure 1(b). The material properties are displayed in table 1, note that three different values of the viscosity are considered and that the Poisson ration ν is taken as zero in order to have a pure 1D problem. The damping factors ξ associated with the values of the viscosities, 10^{-6}s, 10^{-5}s and 10^{-4}s, are 0.393%, 3.93% and 39.3% respectively. In this example, homogeneous initial conditions are considered. The geometry description of the bar and other parameters of the problem are also reported in table 1.

This example focusses in the following quantity of interest:

$$L^{\mathcal{O}}(\mathbf{w}) := \int_I \alpha(t) l^{\mathcal{O}}(\dot{\mathbf{w}}(t))\ \mathrm{d}t,$$

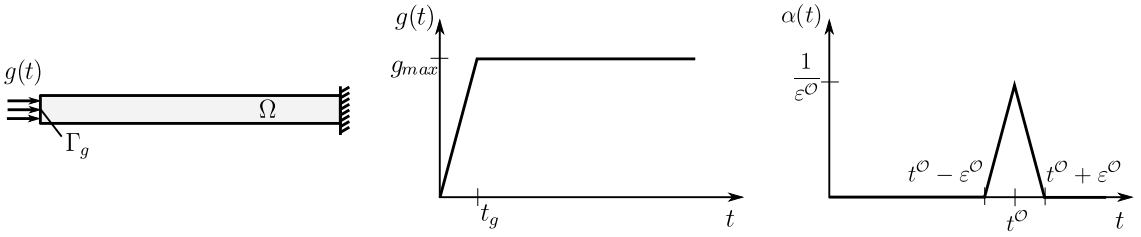

(a) Problem geometry (b) Time dependence of external load (c) Time dependence of the quantity of interest extractor

Figure 1: Example 1: Problem statement and quantity of interest.

Table 1: Example 1: Parameterization

Geometry			Material properties		
Ω	$(0,1)\times(0,0.1)$	m^2	E	$2\cdot 10^{11}$	Pa
Γ_g	$\{0\}\times(0.1)$	m	ν	0	
T	10^{-3}	s	ρ	$8\cdot 10^3$	kg/m^3
			τ	$\{10^{-6}, 10^{-5}, 10^{-4}\}$	s
			ξ	$\{0.393, 3.93, 39.3\}$	%
External load			Quantity of interest		
$g_{\max}$	10^8	Pa	$\varepsilon^{\mathcal{O}}$	$0.05\cdot 10^{-3}$	s
t_g	$0.05\cdot 10^{-3}$	s	$t^{\mathcal{O}}$	$0.65\cdot 10^{-3}$	s

where

$$l^{\mathcal{O}}(\mathbf{w}) = (\mathbf{g}^{\mathcal{O}}, \mathbf{w})_{\Gamma_g},$$

and

$$\mathbf{g}^{\mathcal{O}}(\mathbf{x}) := \frac{-\mathbf{e}_1}{\text{meas}(\Gamma_g)},$$

being $\mathbf{e}_1$ the unit vector in the x–axis. Given the definition of the weighting function $\alpha(t)$ in figure 1(c), the functional $L^{\mathcal{O}}$ represents an average of the velocities at the region of the Neumann boundary Γ_g in the time interval $[t^{\mathcal{O}} - \varepsilon^{\mathcal{O}}, t^{\mathcal{O}} + \varepsilon^{\mathcal{O}}]$.

The numerical simulation is carried out for four different meshes with decreasing element size. The ratio $H/\Delta t$ is kept constant in the refinement processes in order to obtain proper convergence curves (note that if the time step is constant along the

refinement, the error reduction is limited by a threshold given by the time discretization). The quantity kept constant is the ratio $H/\Delta t$ (both H and Δt with the same exponent) because the method used has the same order of convergence both in space and time (linear elements are used in the spatial discretization), see [32] and [33] for the a priori estimates in space and time respectively.

In all computations the time step is taken as $\Delta t = 0.8H/c$, where the scalar $c = \sqrt{E/\rho}$ is the sound speed of the medium. The Newmark parameters are taken as $\beta = 1, \gamma = 0.5$. The number of degrees of freedom, time steps and other parameters related with the discretization are given in table 2. In all the examples, linear triangular meshes are used for computations. The flux-free strategy is used with a reference mesh of element size $h := H/4$. The value of the *exact* solution $\mathbf{u}$ displayed in some figures and tables correspond to the reference solution obtained with the finer mesh (mesh 4).

Table 2: Example 1: Space and time discretizations.

	D.O.F.	H [m]	# elements	N
mesh 1	246	0.0190	160	330
mesh 2	810	0.0095	640	660
mesh 3	2898	0.0047	2560	1320
mesh 4	10914	0.0023	10240	2640

Figure 2 shows the time evolution of the average $l^{\mathcal{O}}(\dot{\mathbf{u}})$ and the weighting function $\alpha(t)$. Note that $L^{\mathcal{O}}(\mathbf{u})$ is directly obtained integrating in time the product of $l^{\mathcal{O}}(\dot{\mathbf{u}})$ and $\alpha(t)$. Note that, figure 2 contains an extra curve corresponding to a pure alastic solution ($\tau = 0$ s). This is a way to illustrate the amount of damping introduced in the computations.

In a first phase, the behavior of the two bounds with respect to 1) the mesh element size and 2) the viscosity of the medium is analyzed. These two parameters are considered because they have a strong influence in the quality of the bounds. Figure 3 and table 3 show the convergence of the bounds for all the values of the viscosity considered in this example. It is observed that the bound gap decreases in the refinement process. This is as expected because the bound gap is directly related with the residual of the numerical solution. On the other hand, the bounds are sharper for the higher values of the viscosity. In fact, the derivation of the bounding properties requires having the viscosity-related parameter τ and therefore the quality of the bounds is degraded if τ tends to zero.

Figure 4 displays the convergence rate of the bound gap and the error $L^{\mathcal{O}}(\hat{\mathbf{e}})$. Note

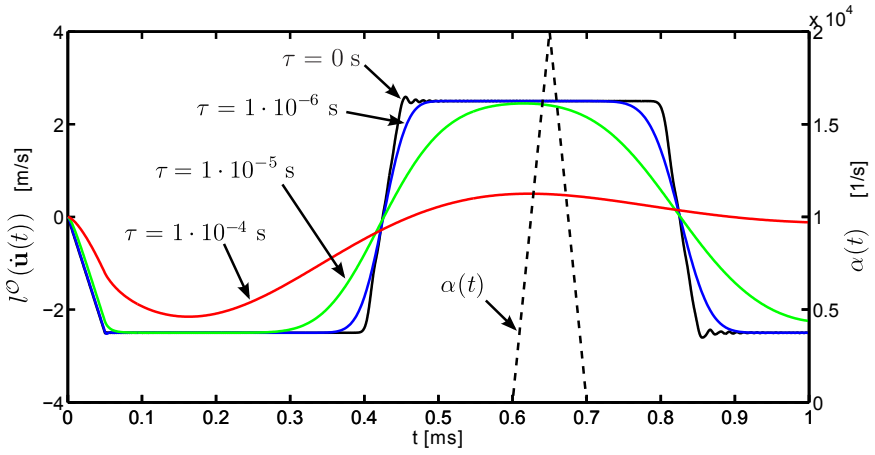

Figure 2: Example 1: Time evolution of the of the average $l^{\mathcal{O}}(\dot{\mathbf{u}}(t))$ for three values of the viscosity (left y-axis) and time evolution of the weighting function $\alpha(t)$ (right y-axis).

Table 3: Example 1: Convergence of the computed quantity of interest and the computed bounds. Results in [m/s].

τ [s]	D.O.F.	$L^{\mathcal{O}}(\hat{\mathbf{u}})$	$L^{\mathcal{O}}(\mathbf{u})$	$\frac{\zeta_{\mathrm{U}}}{L^{\mathcal{O}}(\mathbf{u})}$	$\frac{\zeta_{\mathrm{L}}}{L^{\mathcal{O}}(\mathbf{u})}$	$\frac{\zeta_{\mathrm{U}}^{\mathrm{C-S}}}{L^{\mathcal{O}}(\mathbf{u})}$	$\frac{\zeta_{\mathrm{L}}^{\mathrm{C-S}}}{L^{\mathcal{O}}(\mathbf{u})}$
$1 \cdot 10^{-6}$	246	2.499898	2.499999	1.906818	0.112661	2.794118	-0.794196
	810	2.500008	2.499999	1.220276	0.779112	1.441168	0.558840
	2898	2.499999	2.499999	1.055171	0.944885	1.110285	0.889714
	10914	2.499999	2.499999	1.013780	0.986224	1.027555	0.972444
$1 \cdot 10^{-5}$	246	2.389878	2.389779	1.023540	0.968521	1.055623	0.945586
	810	2.389811	2.389779	1.005730	0.992021	1.013863	0.986444
	2898	2.389786	2.389779	1.001439	0.997990	1.003486	0.996589
	10914	2.389779	2.389779	1.000359	0.999496	1.000872	0.999145
$1 \cdot 10^{-4}$	246	0.484727	0.484657	1.001518	0.997216	1.004156	0.995553
	810	0.484674	0.484657	1.000397	0.999259	1.001101	0.998825
	2898	0.484661	0.484657	1.000099	0.999808	1.000280	0.999697
	10914	0.484657	0.484657	1.000023	0.999949	1.000068	0.999922

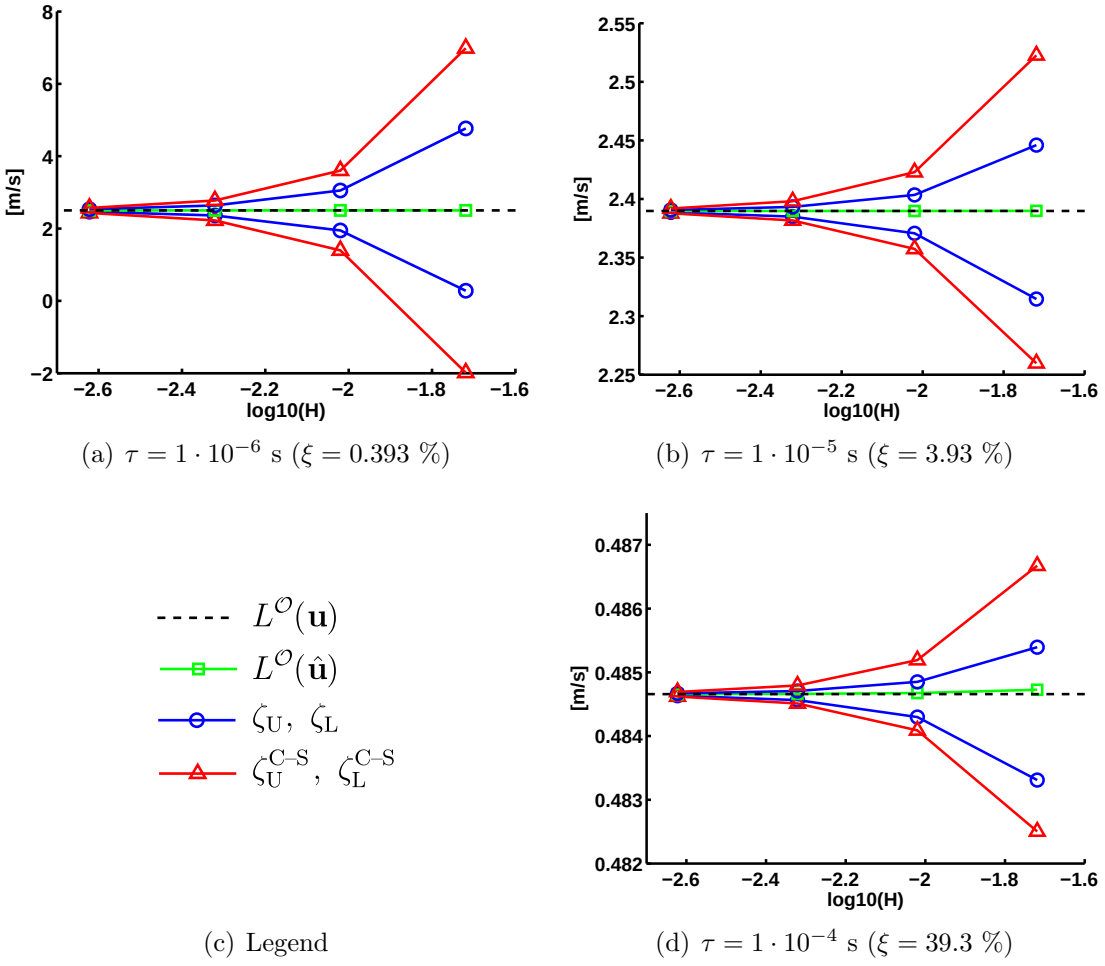

(a) $\tau = 1 \cdot 10^{-6}$ s ($\xi = 0.393$ %)

(b) $\tau = 1 \cdot 10^{-5}$ s ($\xi = 3.93$ %)

(c) Legend

(d) $\tau = 1 \cdot 10^{-4}$ s ($\xi = 39.3$ %)

Figure 3: Example 1: Convergence of the computed bounds for different values of element size and viscosity.

that the obtained rate for the bound gap (slope 2 with respect to the element size) is consistent with the expected value, that corresponds to twice the expected convergence rate for the energy of the error (1 for linear elements). Note that the quality of the bounds increases as long as the mesh is refined or the viscosity increases. The bounds are also improved when the proposed bounding expression (57) is considered instead of the one based on the Cauchy-Schwarz inequality (47).

Note that, the bound gap is theoretically an upper bound of the error $L^{\mathcal{O}}(\hat{\mathbf{e}})$. It is observed in figure 4 that the computed bound gap is indeed a true upper bound, but it strongly overestimates the error. The smaller is the parameter τ, the less accurate is

this upper bound.

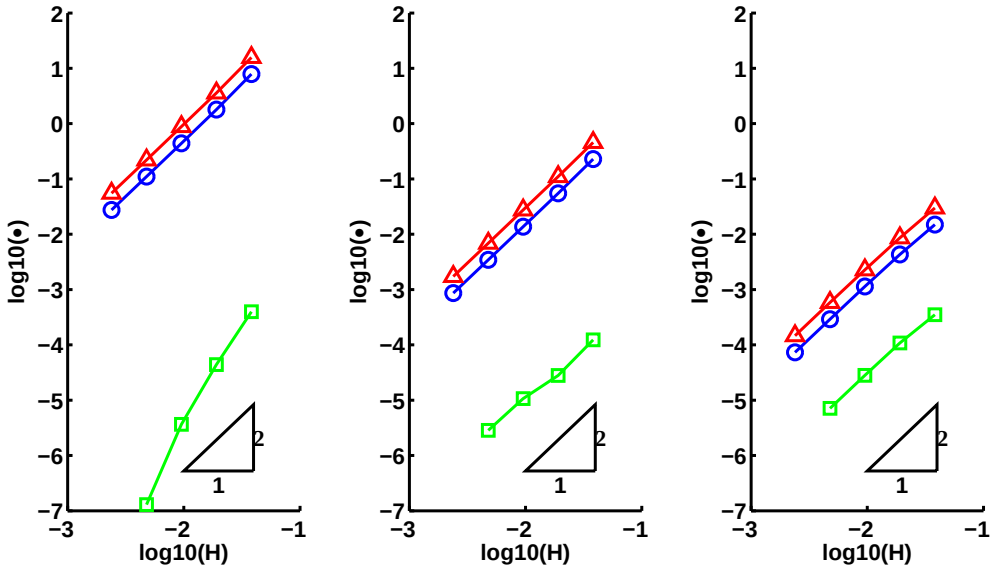

(a) $\tau = 1 \cdot 10^{-6}$ s ($\xi = 0.393$ %) (b) $\tau = 1 \cdot 10^{-6}$ s ($\xi = 3.93$ %) (c) $\tau = 1 \cdot 10^{-6}$ s ($\xi = 39.3$ %)

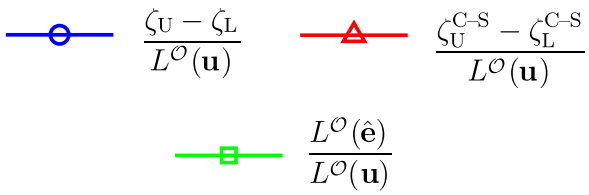

Figure 4: Example 1: Convergence of the computed bound gap and the reference error for different values of element size and viscosity.

As it is previously stated , the bounds ζ_U and ζ_U are computed using asymptotic estimates which are based on a reference mesh. Table 4 shows the influence of considering two different element sizes for the reference mesh. These sizes are, on the one hand, $h := H/4$ which is the reference mesh size considered as the standard choice in this example and, on the other hand, $h := H/8$. The results for both element sizes agree in one significant digit for the coarsest mesh and in three significant digits for the finest mesh. The smaller is the reference size h the larger is the bound gap. This is a standard for e asymptotic estimates. Note that in all cases the computed values are true bounds with respect the reference value $L^{\mathcal{O}}(\mathbf{u}) = 2.389779$ m/s independently of the considered reference mesh size.

Table 4: Example 1: Influence of the reference mesh element size in the computed bounds for $\tau = 1{\cdot}10^{-5}$ s. Results in [m/s].

D.O.F.	ζ_{L} for $h := H/4$	ζ_{L} for $h := H/8$	ζ_{U} for $h := H/4$	ζ_{U} for $h := H/8$
246	2.314553383	2.275610548	2.446035694	2.474136312
810	2.370712445	2.360881927	2.403474732	2.410236611
2898	2.384977566	2.382535545	2.393218595	2.394892692
10914	2.388575410	2.387970113	2.390638593	2.391053021

In a second phase, the origin of the poor quality of the bounds based on the Cauchy-Schwarz inequality is investigated. The goal is to analyze the loss of effectivity introduced by each mathematical manipulation involved in the derivation of the bounds. Three steps are identified in the process of obtaining the bounds that correspond to the successive relations between the four terms below:

$$\begin{aligned} |L^{\mathcal{O}}(\hat{\mathbf{e}}) + \hat{\alpha}| &\lesssim |\!|\!| \hat{\boldsymbol{\sigma}}^{\mathrm{d,ref}} - \mathbf{s}^{\mathrm{E}}(\hat{\mathbf{u}}^{\mathrm{d}}) + \mathbf{s}^{\nu}(\hat{\mathbf{u}}^{\mathrm{d}}) |\!|\!|_{\sigma} |\!|\!| \hat{\mathbf{e}} |\!|\!| \\ &\lesssim |\!|\!| \hat{\boldsymbol{\sigma}}^{\mathrm{d,ref}} - \mathbf{s}^{\mathrm{E}}(\hat{\mathbf{u}}^{\mathrm{d}}) + \mathbf{s}^{\nu}(\hat{\mathbf{u}}^{\mathrm{d}}) |\!|\!|_{\sigma} |\!|\!| \hat{\boldsymbol{\sigma}}^{\mathrm{ref}} - \mathbf{s}(\hat{\mathbf{u}}) |\!|\!|_{\sigma} \\ &\leq |\!|\!| \hat{\boldsymbol{\sigma}}^{\mathrm{d,ff}} - \mathbf{s}^{\mathrm{E}}(\hat{\mathbf{u}}^{\mathrm{d}}) + \mathbf{s}^{\nu}(\hat{\mathbf{u}}^{\mathrm{d}}) |\!|\!|_{\sigma} |\!|\!| \hat{\boldsymbol{\sigma}}^{\mathrm{ff}} - \mathbf{s}(\hat{\mathbf{u}}) |\!|\!|_{\sigma} \end{aligned} \quad (58)$$

The first step corresponds to equation (46) and is related with the use of the Cauchy-Schwarz inequality. The second step corresponds to using the upper bound property of the constitutive relation error, see equation (24). The third step is associated with the overestimation introduced by the flux-free estimate, see (34). The symbol $\lesssim$ indicates that upper bound is not strict but asymptotic. Note that only the last term is actually computable in a practical case. Nevertheless, in this academic example, the reference stresses $\hat{\boldsymbol{\sigma}}^{\mathrm{ref}}$ and $\hat{\boldsymbol{\sigma}}^{\mathrm{d,ref}}$ and the reference version of the error $\hat{\mathbf{e}}$ can also be computed, taking a reference mesh size and time step as $h := H/4$ and $\delta t = \Delta t/4$.

Figure 5 displays the convergence curves of the values in expression (58) for all values of the viscosity considered in this example. Note that most of the effectivity is lost after the application of Cauchy-Schwarz. The introduction of the constitutive relation error also strongly deteriorates the effectivity for the lowest value of the viscosity. The flux-free technique does not seriously deteriorate the effectivity compared to the other steps.

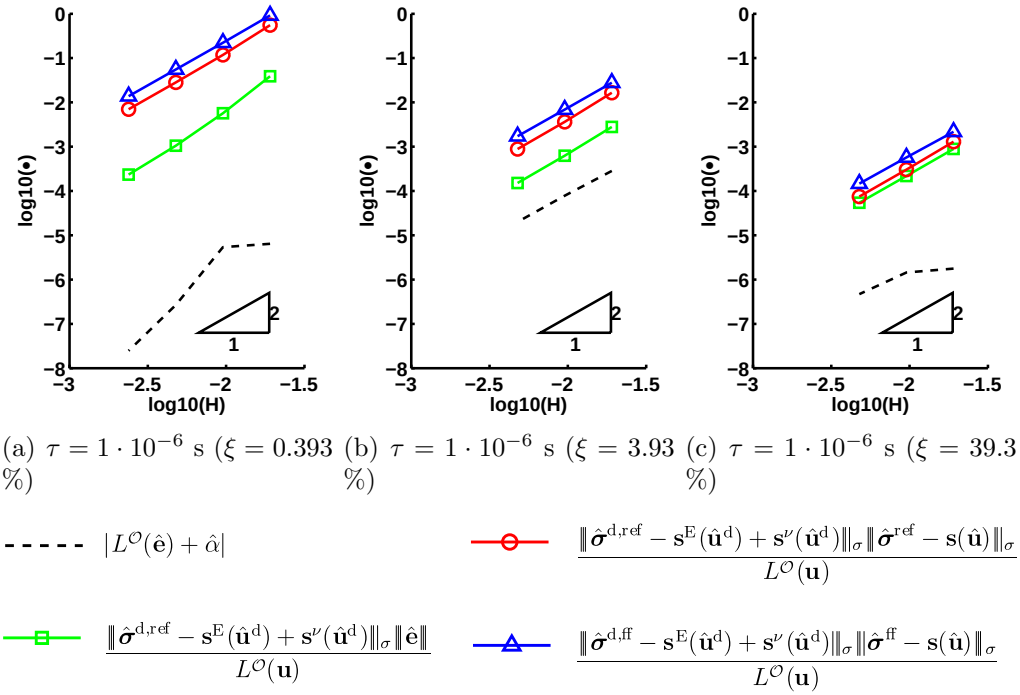

(a) $\tau = 1 \cdot 10^{-6}$ s ($\xi = 0.393$ %) (b) $\tau = 1 \cdot 10^{-6}$ s ($\xi = 3.93$ %) (c) $\tau = 1 \cdot 10^{-6}$ s ($\xi = 39.3$ %)

Figure 5: Example 1: Analysis of the loss of effectivity for the bounds based on the Cauchy-Schwarz inequality. The plotted curves are associated with the error measures appearing in equation (58).

6.2. Example 2: 2D plate

The second numerical example illustrates the performance of the bounds in a full 2D problem. This example is inspired in one from [34]. It consists of a rectangular plate initially at rest which is loaded with two impulsive tractions, see figure 6. This action generates elastic waves propagating along the plate and reaching to the region of interest $\Omega^{\mathcal{O}}$. The quantity of interest is an average of velocities in this region during a time interval (selected such that the wave is noticeable in this region, see figure 7). This quantity is defined as

$$L^{\mathcal{O}}(\mathbf{w}) := \int_I \alpha(t) l^{\mathcal{O}}(\dot{\mathbf{w}}(t)) \, \mathrm{d}t,$$

where

$$l^{\mathcal{O}}(\mathbf{w}) := (\mathbf{f}^{\mathcal{O}}, \mathbf{w}),$$

and

$$\mathbf{f}^{\mathcal{O}}(\mathbf{x}) := \begin{cases} \dfrac{-\mathbf{e}_2}{\mathrm{meas}(\Omega_{\mathcal{O}})} & \mathbf{x} \in \Omega_{\mathcal{O}} \\ \mathbf{0} & \text{else} \end{cases}.$$

Vector $\mathbf{e}_2$ is the unit vector in the y–axis and $\alpha(t)$ is defined in figure 6(c). All the parameters involved in the problem are specified in table 5.

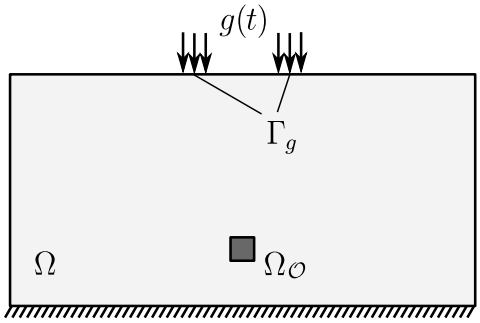

(a) Problem geometry

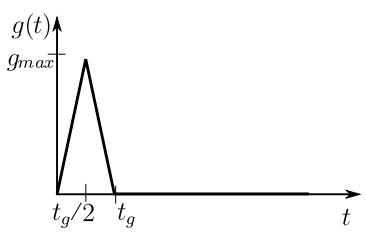

(b) Time dependence of external load

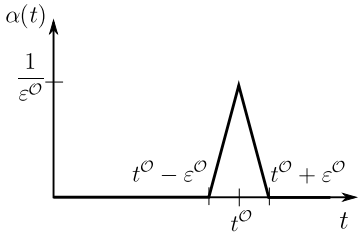

(c) Time dependence of the quantity of interest extractor

Figure 6: Example 2: Problem statement and quantity of interest.

The problem is solved with three different meshes with decreasing element size, see table 6. In all cases linear triangles are considered. The time step is chosen such that $\Delta t = 0.8H/c$. The reference mesh for the flux-free method is taken as $h := H/4$. The value of the *exact* solution $\mathbf{u}$ displayed in some figures and tables correspond to the reference solution obtained with the finer mesh (mesh 3) Other parameters related with the discretization are given in table 6.

Several snap shots of the numerical solution of the original and adjoint problems are shown in figures 8, 9 and 10 for the three values of the viscosity under consideration.The damping factors ξ associated with the values of the viscosity parameter, 10^{-4}s, 10^{-3}s and 10^{-2}s, are 0.0247%, 0.247% and 2.47% respectively. Note that for the original problem the elastic waves propagate forward in time, and backward in time for the adjoint.

Figure 11 shows the computed value $L^{\mathcal{O}}(\hat{\mathbf{u}})$ and the bounds obtained for the three values of the viscosity and decreasing element size. In addition, table 7 shows the effectivity of the computed bounds. Note that in this case the bounds are also sharper for higher

Table 5: Example 2: Parameterization

Geometry			Material properties		
Ω	$(-0.5, 0.5) \times (0, 0.5)$	m^2	E	$8/3$	Pa
$\Omega_{\mathcal{O}}$	$(-0.025, 0.025) \times (0.1, 0.15)$	m^2	ν	$1/3$	
Γ_g	$[(0.075, 0.125) \cup (-0.075, -0.125)] \times (0.5)$	m	ρ	1	kg/m^3
T	0.25	s	τ	$\{10^{-4}, 10^{-3}, 10^{-2}\}$	s
			ξ	$\{0.0247, 0.247, 2.47\}$	%
External load			**Quantity of interest**		
$g_{\max}$	30	Pa	$\varepsilon^{\mathcal{O}}$	0.01	s
t_g	0.005	s	$t^{\mathcal{O}}$	0.2170	s

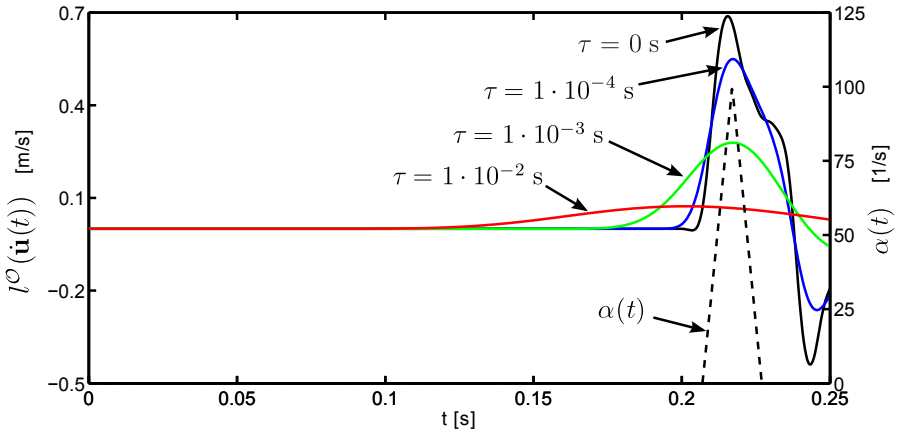

Figure 7: Example 2: Time evolution of the of the average $l^{\mathcal{O}}(\dot{\mathbf{u}}(t))$ for three values of the viscosity (left y-axis) and time evolution of the weighting function $\alpha(t)$ (right y-axis).

values of τ and for smaller element sizes. In particular, for $\tau = 10^{-4}$s and $\tau = 10^{-3}$s the bounds are not sharp at all, even for mesh number 3, which can be considered an overkill mesh. Note that, in these two cases, the bounds do not allow identifying which is the sign of the quantity of interest. For $\tau = 10^{-2}$s the bounds are much sharper. The proposed bounds reduce in approximately 50% the bound gap with respect to the ones based on the Cauchy-Schwarz inequality, in all cases. Note however that for the small

Table 6: Example 2: Space and time discretizations.

	D.O.F.	H [mm]	# elements	N
mesh 1	24000	0.16	23596	325
mesh 2	95190	0.08	94384	650
mesh 3	379146	0.04	377536	1300

values of the viscosity, $\tau = 10^{-4}$s and $\tau = 10^{-3}$s, this reduction is not sufficient to have bounds applicable in practical engineering examples.

Table 7: Example 2: Convergence of the computed bounds. Results in [m/s].

τ [s]	D.O.F.	$L^{\mathcal{O}}(\hat{\mathbf{u}})$	$L^{\mathcal{O}}(\mathbf{u})$	$\frac{\zeta_{\mathrm{U}}}{L^{\mathcal{O}}(\mathbf{u})}$	$\frac{\zeta_{\mathrm{L}}}{L^{\mathcal{O}}(\mathbf{u})}$	$\frac{\zeta_{\mathrm{U}}^{\mathrm{C–S}}}{L^{\mathcal{O}}(\mathbf{u})}$	$\frac{\zeta_{\mathrm{L}}^{\mathrm{C–S}}}{L^{\mathcal{O}}(\mathbf{u})}$
$1 \cdot 10^{-4}$	24000	0.4937	0.4960	110.0524	-113.8099	224.8397	-222.8850
	95190	0.4932	0.4960	32.1210	-31.5976	64.7088	-62.7284
	379146	0.4960	0.4960	9.2333	-7.6063	17.8371	-15.8420
$1 \cdot 10^{-3}$	24000	0.2681	0.2697	6.5943	-4.8098	12.4183	-10.3898
	95190	0.2681	0.2697	2.5800	-0.6352	4.2187	-2.2117
	379146	0.2697	0.2697	1.4224	0.5637	1.8595	0.1422
$1 \cdot 10^{-2}$	24000	0.0668	0.0672	1.6457	0.3498	2.2953	-0.2967
	95190	0.0668	0.0672	1.1867	0.8121	1.3745	0.6252
	379146	0.0672	0.0672	1.0520	0.9477	1.1043	0.8956

7. Conclusion

Bounds for linear functional outputs are derived for linear visco-elastodynamics. A new bounding expression is presented which improves the quality with respect to the previous approaches based on the Cauchy-Schwarz inequality. The proposed new approach is based on an alternative error representation, involving symmetrized error equations, which is derived precluding the use of the Cauchy-Schwarz inequality.

The key ingredient for the practical application of the method is the construction of admissible fields for both the original and adjoint problems. The proposed formulation is valid for any numerical method, provided that the numerical solution furnishes admissible fields (possibly after some post processing). Here, the K-admissible field is computed as a post process of the Newmark solution. On the other hand, the D-admissible field is computed with the asymptotic flux-free strategy. This method is based on a reference mesh and therefore, the proposed bounds hold when the element size of the reference mesh is fine enough. In practice, the numerical examples show that the computed values are indeed true bounds of the quantity of interest.

All the developments in the paper require that the formulation includes a certain amount of viscosity. In the present case, the linear Kelvin-Voigt model is considered. The quality of the results obtained degenerate in the limit case of elasticity (zero or very small viscosity). In materials with small amounts of viscosity, the bounds obtained are pessimistic. The numerical tests reveal that when the meshes are refined the bound gap tends to be reduced and, correspondingly, the strategy provides sharp bounds for fine enough meshes. Nevertheless, in practice, for low viscosity, the meshes providing accurate bounds are not computationally affordable. Therefore, further research is needed to explore alternative pertinent bounds for nearly elastic problems.

Appendix A. Non-homogeneous Dirichlet conditions

It is well known that non-homogeneous Dirichlet conditions does not introduce any extra conceptual difficulty. In the case of non homogeneous Dirichlet conditions it suffices to define an arbitrary (and easy to produce) function $\boldsymbol{\psi}$ fulfilling them, that is such that $\boldsymbol{\psi} = \mathbf{u}_{\mathrm{D}}$ on $\Gamma_{\mathrm{D}} \times I$. Once $\boldsymbol{\psi}$ is available, the analysis is done for function $\mathbf{u}^* := \mathbf{u} - \boldsymbol{\psi}$ fulfilling homogeneous conditions, $\mathbf{u}^* = \mathbf{0}$ on $\Gamma_{\mathrm{D}} \times I$. Note that, function $\mathbf{u}^* \in \boldsymbol{\mathcal{U}}$ fulfills the weak form

$$B(\mathbf{u}^*, \mathbf{w}) = L^*(\mathbf{w}) \quad \forall \mathbf{w} \in \boldsymbol{\mathcal{W}},$$

where $L^*(\mathbf{w}) := L(\mathbf{w}) - B(\boldsymbol{\psi}, \mathbf{w})$ and equivalently, the strong form

$$\begin{aligned}
\rho \ddot{\mathbf{u}}^* - \boldsymbol{\nabla} \cdot \boldsymbol{\sigma}(\mathbf{u}^*) &= \mathbf{f} - \rho \ddot{\boldsymbol{\psi}} - \boldsymbol{\nabla} \cdot \boldsymbol{\sigma}(\boldsymbol{\psi}) \quad \text{in } \Omega \times I, \\
\mathbf{u}^* &= \mathbf{0} \quad \text{on } \Gamma_{\mathrm{D}} \times I, \\
\boldsymbol{\sigma}(\mathbf{u}^*) \cdot \mathbf{n} &= \mathbf{g} - \boldsymbol{\sigma}(\boldsymbol{\psi}) \cdot \mathbf{n} \quad \text{on } \Gamma_{\mathrm{N}} \times I, \\
\mathbf{u}^* &= \mathbf{u}_0 - \boldsymbol{\psi} \quad \text{at } \Omega \times \{0\}, \\
\dot{\mathbf{u}}^* &= \mathbf{v}_0 - \dot{\boldsymbol{\psi}} \quad \text{at } \Omega \times \{0\}.
\end{aligned}$$

Thus, the non-homogeneous conditions are easily reduced to homogeneous adding some correction terms to the forcing data of the original problem.

Function $\boldsymbol{\psi}$ can be builded using the shape functions of the computational mesh

$$\boldsymbol{\psi}(\mathbf{x},t) := \sum_{i \in \mathcal{N}_{\mathrm{D}}} N_i(\mathbf{x}) \mathbf{u}_{\mathrm{D}}(\mathbf{x}_i,t), \tag{A.1}$$

where $\mathcal{N}_{\mathrm{D}}$ is the set of indices of nodes lying on the Dirichlet boundary Γ_{D} and $\mathbf{x}_i$ is the position of the i-th node. Note that $\boldsymbol{\psi}$ has to be such that $\boldsymbol{\psi} \in \boldsymbol{\mathcal{U}}$ (H^1 in space and H^2 in time) in order to properly define L^*. The regularity in space is guaranteed by the shape functions. The regularity in time should be provided by the Dirichlet condition $\mathbf{u}_{\mathrm{D}}$. That is, $\mathbf{u}_{\mathrm{D}}$ has to be such that $\mathbf{u}_{\mathrm{D}}(\mathbf{x},\cdot) \in [H^2(I)]^d$ for all $\mathbf{x} \in \Gamma_{\mathrm{D}}$.

Acknowledgement

Partially supported by Ministerio de Educación y Ciencia, Grant DPI2011-27778-C02-02 and Univeritat Politècnica de Catalunya (UPC-BarcelonaTech), Grant UPC-FPU. The support of the Col·legi d'Enginyers de Camins, Canals i Ports (Catalunya) is also greatfuly acknowledged.

References

[1] I. Babuŝka, W. Rheinboldt, Error estimates for adaptive finite element computations, SIAM J. Numer. Anal. 18 (1978) 736–754.

[2] P. Ladevèze, D. Leguillon, Error estimate procedure in the finite element method, SIAM J. on Numerical Analysis 20 (1983) 485–509.

[3] O. Zienkiewicz, J. Zhu, A simple error estimator and adaptative procedure for practical engineering analysis, Int. J. Numer. Meth. Engrg. 24 (1987) 337–357.

[4] M. Paraschivoiu, J. Peraire, A. Patera, A posteriori finite element bounds for linear-functional outputs of elliptic partial differential equations, Comput. Methods Appl. Mech. Engrg. 150 (1997) 289–321.

[5] N. Parés, J. Bonet, A. Huerta, J. Peraire, The computation of bounds for linear-functional outputs of weak solutions to the two-dimensional elasicity equations, Comput. Methods Appl. Mech. Engrg. 195 (2006) 406–429.

[6] F. Cirak, E. Ramm, A posteriori error estimation and adaptivity for linear elasticity using the reciprocal theorem, Comput. Methods Appl. Mech. Engrg. 156 (1998) 351–362.

[7] S. Prudhomme, J. Oden, On goal-oriented error estimation for elliptic problems: application to the control of pointwise errors, Comput. Methods Appl. Mech. Engrg. 176 (1999) 313–331.

[8] D. Aubry, D. Lucas, B. Tie, Adaptive strategy for transient/coupled problems. Applications to thermoelasticity and elastodynamics, Comput. Methods Appl. Mech. Engrg. 176 (1999) 41–50.

[9] X. Li, N. Wiberg, Implementation and adaptivity of a space-time finite element method for structural dynamics, Comput. Methods Appl. Mech. Engrg. 156 (1998) 211–229.

[10] N. Wiberg, X. Li, Adaptive finite element procedures for linear and non-linear dynamics, Int. J. Numer. Meth. Engrg. 46 (1999) 178–1802.

[11] L. Chamoin, P. Ladevèze, A non-intrusive method for the calculation of strict and efficient bounds of calculated outputs of interest in linear viscoelasticity problems, Comput. Methods Appl. Mech. Engrg. 197 (2008) 994–1014.

[12] J. Combe, P. Ladevèze, J. Pelle, Discretization error estimator for transcient dynamic simulations, Advances in Engrg. Software 33 (2002) 553–563.

[13] J. Combe, P. Ladevèze, J. Pelle, Constitutive relation error estimator for transient finite element analysis, Comput. Methods Appl. Mech. Engrg. 176 (1999) 165–185.

[14] P. Ladevèze, J. Pelle, Estimation of discretization errors in dynamics, Computers and Structures 81 (2003) 1133–1148.

[15] A. Schleupen, E. Ramm, Local and global error estimations in linear structural dynamics, Computers and structures 76 (2000) 741–756.

[16] D. Fuentes, D. Littlefiel, J. dOden, S. Prudhomme, Extensions of goal-oriented error estimation methods to simulation of highly-nonlinear response of shock-loaded elastomer-reinforced structures, Comput. Methods Appl. Mech. Engrg. 195 (2006) 4659–4680.

[17] P. Ladevèze, J. Waeytens, Model verification in dynamics trough strict upper bounds, Comput. Methods Appl. Mech. Engrg. 198 (2009) 1775–1784.

[18] J. Waeytens, Contrôle des calculs en dynamique: bornes strictes et pertinents sur une quantié d'intérêt, Ph.D. thesis, LMT-Cachan (2010).

[19] P. Ladevèze, Strict upper error bounds for computed outputs of interest in computational structural mechanics, Computational Mechanics 42 (2008) 271–286.

[20] J. Waeytens, L. Chamoin, P. Ladevèze, Guaranteed error bounds on pointwise quantities of interest for transient viscodynamics problems, Computational Mechanics 49 (2012) 291–307.

[21] N. Parés, P. Díez, A. Huerta, Bounds of functional outputs for parabolic problems. Part I: Exact bounds of the discontinuous galerkin time discretization, Comput. Methods Appl. Mech. Engrg. 197 (2008) 1641–1660.

[22] N. Parés, P. Díez, A. Huerta, A subdomain-based flux-free a posteriori error estimators, Comput. Methods Appl. Mech. Engrg. 195 (2006) 297–323.

[23] N. Newmark, A method of computation for structural dynamics, J. of Engineering Mechanics 85 (1959) 67–94.

[24] J. Hughes, M. Hulbert, Space-time finite element methods for elastodynamics: Formulations and error estimates, Comput. Methods Appl. Mech. Engrg. 66 (1988) 339–363.

[25] M. Hulbert, J. Hughes, Space-time finite element methods for second-order hypeerbolic equations, Comput. Methods Appl. Mech. Engrg. 84 (1990) 327–348.

[26] P. Ladevèze, J. Pelle, La maîtrise du calcul en mécanique linéaire et non linéaire, Lavoisier, 2001.

[27] M. Ainsworth, J. Oden, A posteriori error estimation in Finite element analysis, John Wiley & Sons Ltd., 2000.

[28] R. Cottereau, P. Díez, A. Huerta, Strict error bounds for linear solid mechanics problems using a subdomain-based flux-free method, Comput. Mech. 44 (2009) 533–547.

[29] J. P. Moitinho de Almeida, O. J. B. Almeida Pereira, Upper bounds of the error in local quantities using equilibrated and compatible finite element solutions for linear elastic problems, Comput. Methods Appl. Mech. Engrg. 195 (2006) 279–296.

[30] O. J. B. Almeida Pereira, J. P. Moitinho de Almeida, Dual adaptive finite element refinement for multiple local quantities in linear elastostatics, Int. J. Numer. Meth. Engrg. 83 (2010) 347–365.

[31] J. Oden, S. Prudhomme, Goal-oriented error estimation and adaptivity for the finite element method, Computers and Math. with Appl. 41 (2001) 735–765.

[32] C. Johnson, Numerical solution of partial differential equations by the finite element method, Cambridge University Press, 1990.

[33] P. Raviart, J. Thomas, Introduction à l'analysie numérique des équations aux dérivées partielles, Masson, 1983.

[34] N. Nguyen, J. Peraire, B. Cockburn, High-order implicit hybridizable discontinuous Galerkin methods for acoustics and elastodynamics, Journal of Computational Physics 230 (2011) 3695–3718.

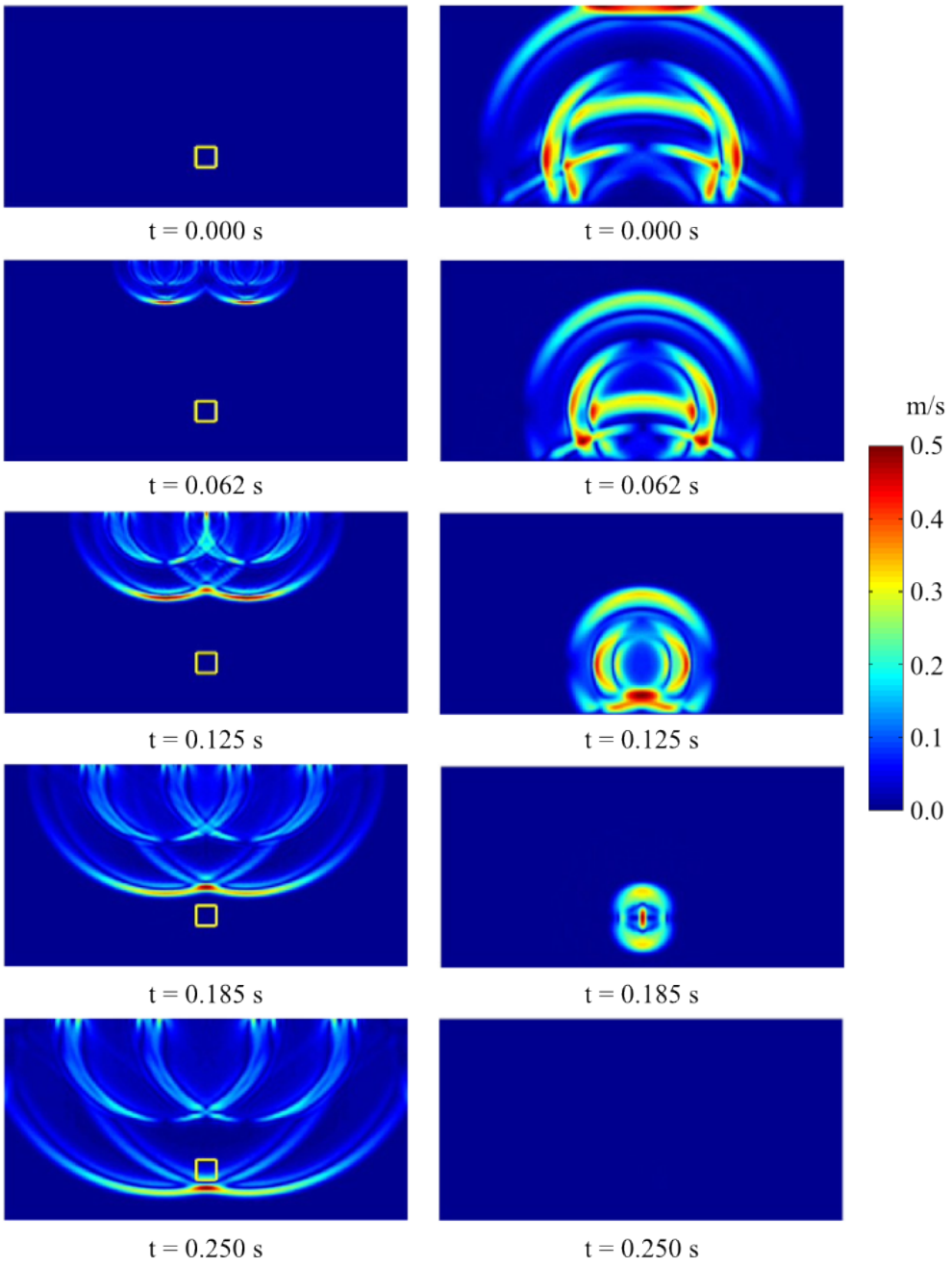

Figure 8: Example 2: Magnitude of the original (left) and adjoint (right) velocities for $\tau = 10^{-4}$ s ($\xi = 0.0247\%$).

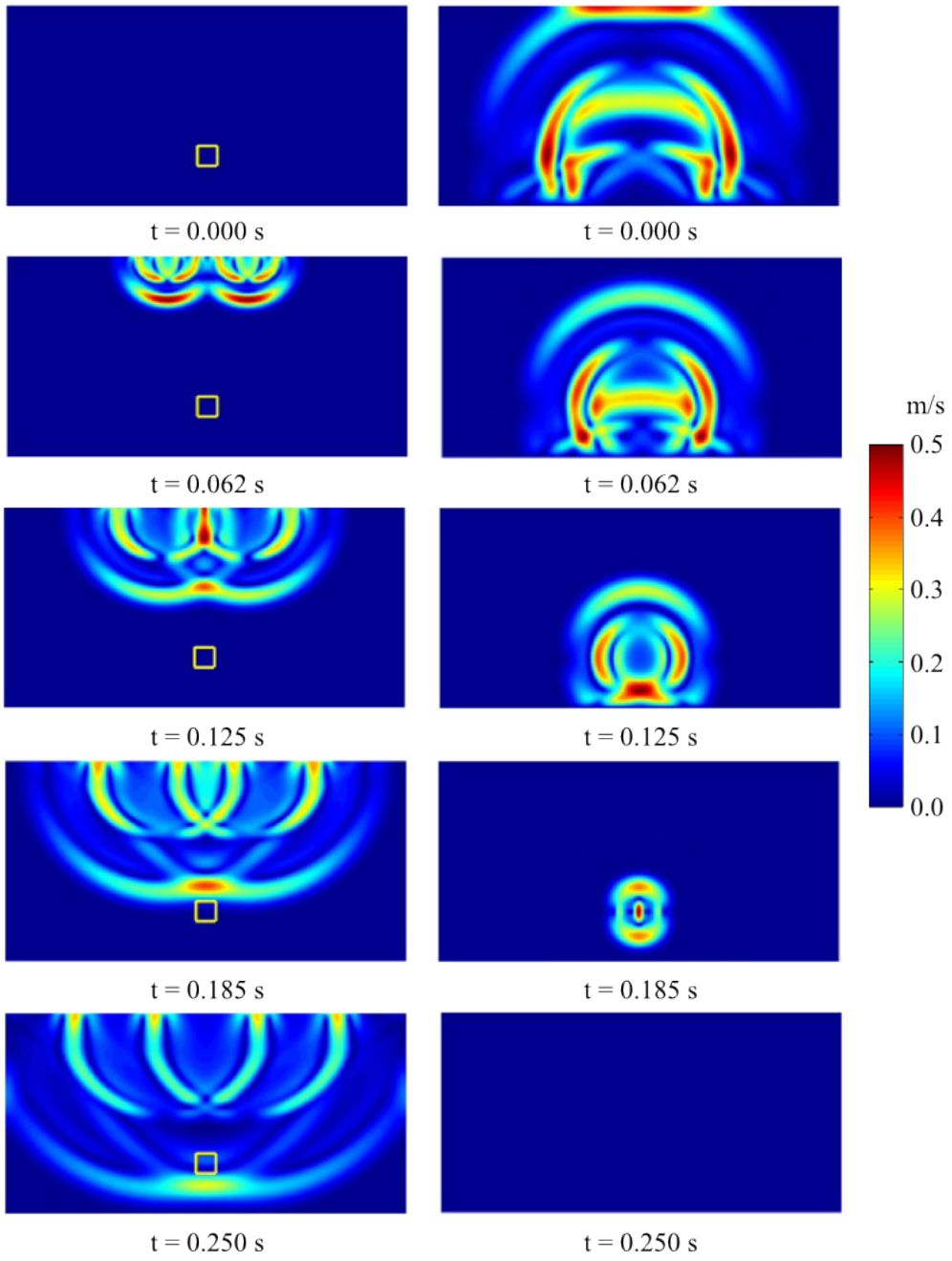

Figure 9: Example 2: Magnitude of the original (left) and adjoint (right) velocities for $\tau = 10^{-3}$ s ($\xi = 0.247\%$).

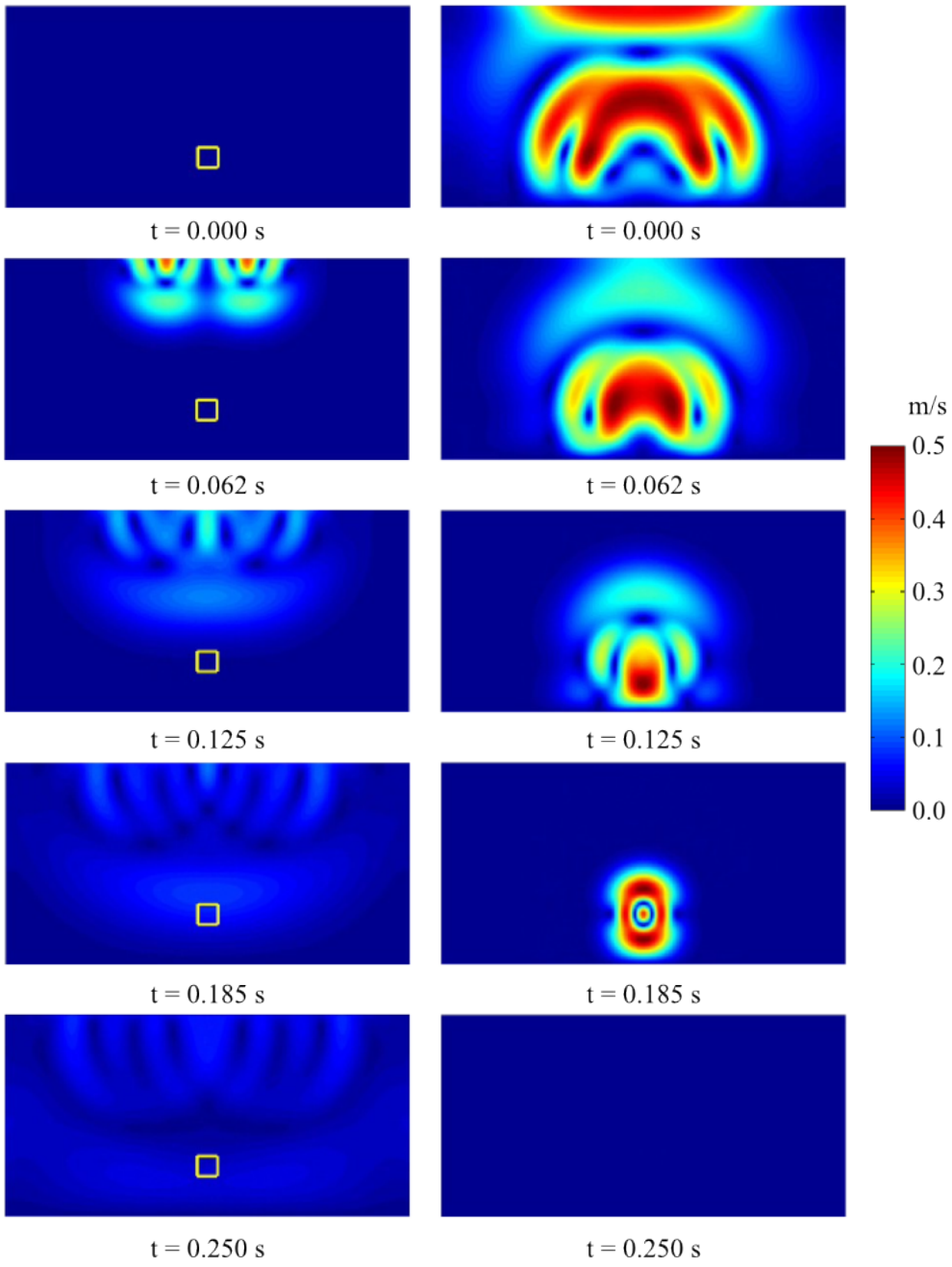

Figure 10: Example 2: Magnitude of the original (left) and adjoint (right) velocities for $\tau = 10^{-2}$ s $\xi = (2.47\%)$.

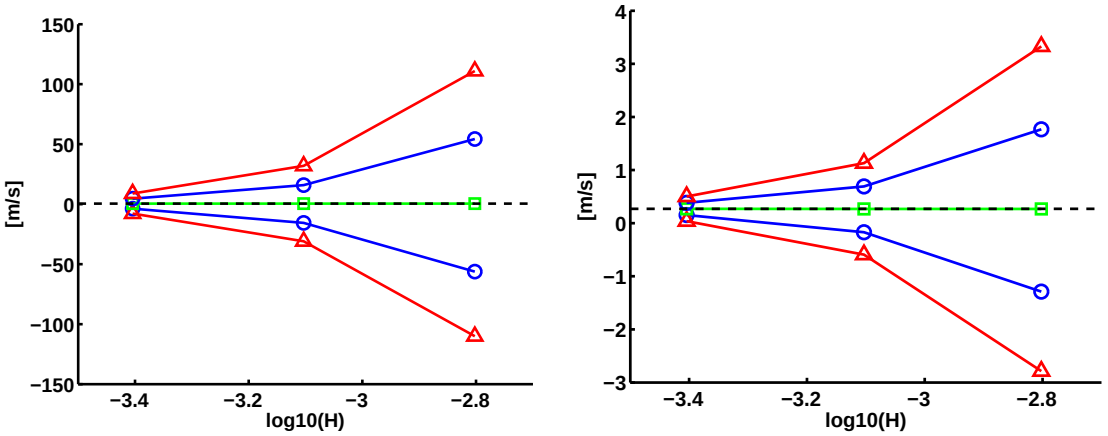

(a) $\tau = 1 \cdot 10^{-6}$ s ($\xi = 0.0247\%$)

(b) $\tau = 1 \cdot 10^{-5}$ s ($\xi = 0.247\%$)

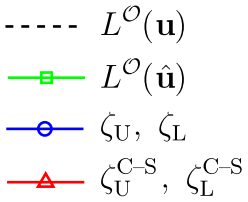

(c) Legend

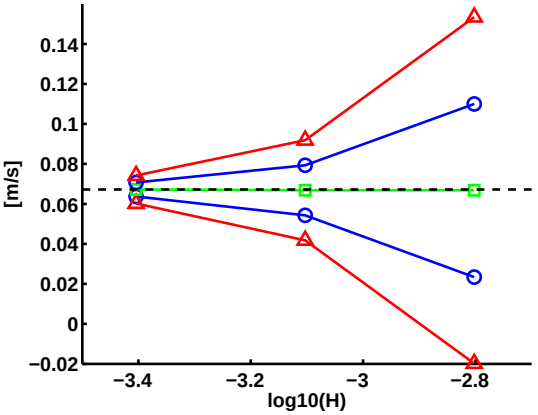

(d) $\tau = 1 \cdot 10^{-4}$ s ($\xi = 2.47\%$)

Figure 11: Example 2: Convergence of the computed bounds for different values of element size and viscosity.